Mixed Regioselectivity in the Arg-177 Mutants of *Corynebacterium diphtheriae* Heme Oxygenase as a Consequence of in-Plane Heme Disorder†

Yuhong Zeng,‡,§ Rahul Deshmukh,§,|| Gregori A. Caignan,‡ Richard A. Bunce,⊥ Mario Rivera,*,‡ and Angela Wilks*,||

Department of Chemistry, The University of Kansas, 1251 Wescoe Hall Drive, Lawrence, Kansas 66045-7582, Department of Chemistry, Oklahoma State University, Stillwater, Oklahoma 74078-3071, and Department of Pharmaceutical Sciences, School of Pharmacy, University of Maryland, Baltimore, Maryland 21201-1180

Received November 5, 2003; Revised Manuscript Received February 19, 2004

ABSTRACT: It has been reported that the R183E and R183D mutants of rat heme oxygenase-1 (r-HO-1) produce approximately 30% δ-biliverdin [Zhou, H., *et al*. (2000) *J. Am. Chem. Soc. 122*, 8311−8312]. Two plausible mechanisms were proposed to explain the observations. (a) Electrostatic repulsion between E183 (D183) and one of the heme propionates forces the heme to rotate, thereby placing the δ-meso carbon in a position that is susceptible to oxidation. (b) Rearrangement of the distal pocket structure is triggered by the formation of a hydrogen bond between E183 (D183) and K179. A change in the pK_a for the $Fe^{III}-H_2O$ to $Fe^{III}-OH$ transition of the mutants was interpreted to be consistent with rearrangement of the hydrogen bond network in the distal pocket. The large similarities between the high-frequency portion of the ^1H NMR spectra corresponding to the wild type and R183E and R183D mutants were interpreted to indicate that the heme in the mutants is not rotated to a significant extent. We have re-examined this issue by studying the corresponding R177 mutants in heme oxygenase from *Corynebacterium diphtheriae* (*cd*-HO). Replacing R177 with E or D results in the formation of approximately 55% α- and 45% δ-biliverdin, whereas the R177A mutant retains α-regioselectivity. In addition, the K13N/Y130F/R177A triple mutant catalyzed the formation of 60% δ- and 40% α-biliverdin, while single mutants K13N and Y130F did not appreciably change the regioselectivity of the reaction. The pK_a of the $Fe^{III}-H_2O$ to $Fe^{III}-OH$ transition in wild-type *cd*-HO is 9.1, and those of the R177E, R177D, R177A, and K13N/Y130F/R177A mutants are 9.4, 9.5, 9.2, and 8.0, respectively. Thus, no obvious correlation exists between the changes in pK_a and the altered regioselectivity. NMR spectroscopic studies conducted with the R177D and R177E mutants of *cd*-HO revealed the presence of three heme isomers: a major (M) and a minor (m) heme orientational isomer related by a 180° rotation about the α−γ meso axis and an alternative seating (m′) which is related to m by an 85° in-plane rotation of the macrocycle. The in-plane rotation of m to acquire conformation m′ is triggered by electrostatic repulsion between the side chains of D or E at position 177 and heme propionate-6. As a consequence, the δ-meso carbon in m′ is placed in the position occupied by the α-meso carbon in m, where it is susceptible to hydroxylation and subsequent formation of δ-biliverdin.

Heme oxygenase (HO) catalyzes the rate-limiting step in the oxidative cleavage of heme to biliverdin, which results in the formation of CO and the release of iron (*1*, *2*). The recently identified bacterial HOs are NADPH-dependent enzymes that catalyze the oxidation of heme by a mechanism similar to that described for the mammalian enzymes (*3*−*5*). The bacterial HO enzymes are critical in the final step of a unique pathway by which pathogenic bacteria utilize heme as an iron source (*6*−*8*).

Although the nature of the stable intermediates in the oxidation of heme to biliverdin has been determined, the role of protein structure in defining characteristics such as ligand discrimination, oxygen activation, and regioselectivity are only just beginning to be understood. The recently published crystal structures of *Neisserriae meningitides* HO (*nm*-HO) (*9*) and human HO-1 (h-HO-1) (*10*) have shown that unlike the globins and peroxidases, HOs do not have a distal histidine or single polar residue that may stabilize a coordinated dioxygen (O_2) or peroxide (^-OOH) ligand. The more recently published crystal structures of h-HO-1 (*11*), *nm*-HO (*9*), and ferrous heme-NO (*12*), as well as the NMR spectroscopic studies conducted with cyanide (*13*−*15*) and hydroxide (*16*) complexes of HO, have shed some light on the role played by the ordered hydrogen bonding network of the distal pocket in facilitating the coordination of the

† This work was supported by NIH Grants GM-50503 (M.R.) and AI-55912 (A.W.).

* To whom correspondence should be addressed. Telephone: (410) 706-2537. Fax: (410) 706-0346. E-mail: awilks@rx.umaryland.edu or mrivera@ku.edu.

‡ The University of Kansas.

§ These authors contributed equally to this work.

⊥ Oklahoma State University.

|| University of Maryland.

10.1021/bi035970o CCC: $27.50
Published on Web 04/14/2004

iron-bound $^{-}$OOH ligand and in the subsequent hydroxylation of the heme.

Insight obtained from the crystal structures of both the mammalian (*10*, *17*) and bacterial enzymes (*9*) suggests that the regioselectivity of the reaction is likely to be controlled by steric interactions between the distal helix and the heme, which would restrict access of the activated $Fe^{III}-OOH$ intermediate to the β-, δ-, and γ-meso carbons. In addition to steric steering, electronic factors have also been implicated in the control of regioselectivity. Modified hemes in which electron-withdrawing and electron-donating substituents located on a given meso carbon were shown to exert a different influence on the regioselectivity of heme cleavage were identified (*18*−*20*). More recently, magnetic resonance studies on model complexes of the low-spin $Fe^{III}-OOH$ species of HO suggest that this key intermediate exists as an equilibrium mixture consisting of a planar heme with a $(d_{xy})^2(d_{xz},d_{yz})^3$ electron configuration (d_π hereafter) and a ruffled heme with a $(d_{xz},d_{yz})^4(d_{xy})^1$ electron configuration [$(d_{xy})^1$ hereafter] (*21*). An important aspect of the $(d_{xy})^1$ electronic ground state is that porphyrin deformation places a large electron spin density at the meso carbons. It was therefore hypothesized that at ambient temperatures the electronic configuration of the heme in HO could be $(d_{xy})^1$; thus, the ruffled heme could be expected to aid attack of the terminal oxygen of the $Fe^{III}-OOH$ oxidizing species (*21*). ^{13}C NMR spectroscopic studies conducted at ambient temperatures with the hydroxide complex ($Fe^{III}-OH$) of heme oxygenase as a model of the hydroperoxide intermediate ($Fe^{III}-OOH$) strongly suggest that the coordination of hydroxide in the distal pocket induces the formation of at least three populations of $Fe^{III}-OH$ complexes with distinct electronic configurations and nonplanar ring distortions (*16*). These findings were interpreted to suggest that if the ligand field strength of the coordinated $^{-}$OOH ligand in HO is modulated by the distal pocket in a manner similar to that seen with $^{-}$OH, the resultant large spin density at the meso carbon and nonplanar deformations of the macrocycle prime the heme to participate actively in its own hydroxylation (*16*). Thus, it is likely that the regioselectivty of heme oxygenation is determined by a combination of both steric and electronic factors.

Interactions between heme propionates and amino acid residues in HO also appear to contribute to the regioselective outcome of heme oxygenation (*22*). For instance, the heme propionates in all α-hydroxylating HO enzymes of known structure exhibit electrostatic and hydrogen bonding interactions with nearby Lys and Tyr side chains. These contacts involve Lys-16 and Tyr-112 in *nm*-HO or the equivalent Lys-18 and Tyr-134 residues in h-HO-1 and r-HO-1. In contrast, the equivalent residues in the δ-hydroxylating heme oxygenase from *Pseudomonas aeruginosa* (*pa*-HO) are Asn-19 and Phe-117, respectively. We have recently demonstrated that the absence of interactions between the heme propionates and the side chains of Asn-19 and Phe-117 in *pa*-HO results in a 100° in-plane rotation of the heme that places the δ-meso carbon in the position typically occupied by the α-meso carbon in the fold of all α-hydroxylating HO enzymes (*22*). Furthermore, when Asn-19 and Phe-117 are mutated to Lys and Tyr, respectively, the heme in the double mutant exhibits a dynamic equilibrium between two heme seatings, related to one another by an ∼100° in-plane rotation. One of these seatings is identical to that seen in wild-type *pa*-HO and conduces to δ-hydroxylation, whereas the second, alternative seating positions the α-meso carbon in the place formerly occupied by the δ-meso carbon, and therefore results in the hydroxylation of the α-meso carbon. This dynamic equilibrium between two heme seatings is consistent with the oxidation of heme to α- and δ-biliverdin catalyzed by the N19K/F117Y double mutant of *pa*-HO (*22*).

Close examination of the crystal structure of the heme−r-HO-1 complex reveals that in addition to Lys-18 and Tyr-134 the side chain of Arg-183 is in a position that favors interactions with the heme propionates (Figure 1A). Studies conducted with the R183E and R183D mutants of r-HO-1 demonstrated that these molecules oxidize heme to produce a mixture of α-biliverdin and δ-biliverdin; the R183E and R183D mutants were reported to form 35% and 20% δ-biliverdin, respectively (*23*). The authors of this study considered the possibility that electrostatic repulsion between E183 or D183 and one of the heme propionates would cause an in-plane rotation of the heme to account for the observed regioselectivity of the R183E and R183D mutants. However, this hypothesis was disfavored by the authors on the basis that the high-frequency portions of the ^{1}H NMR spectra of the wild type and R183 mutants of r-HO-1 are very similar (*23*). Consequently, the authors forwarded an alternative explanation that entails a rearrangement of the distal hydrogen bonding network, whereby the carboxylate of Glu-183 (or Asp-183) interacts with Lys-179, which in turn forms a hydrogen bond with Ser-142. Hence, it was proposed that this alternate hydrogen bonding network would alter the structure of the distal pocket and consequently the regioselectivity of heme oxygenation. These authors proposed that the change in the structure of the distal pocket was manifested in a change in the pK_a value for dissociation of the high-spin aqua ($Fe^{III}-H_2O$) to the low-spin hydroxo ($Fe^{III}-OH$) complex, which is 7.9 for wild-type r-HO-1 and 9.2 for the R183E complex. It is important to point out, however, that the same study reported that the K179A and K179E mutants of r-HO-1, although exhibiting pK_a values (9.6 and 10.6, respectively) different from those of the wild-type enzyme, yield solely the α-isomer. This suggests that changes in regioselectivity are not correlated with changes in pK_a for the $Fe^{III}-H_2O$ to $Fe^{III}-OH$ transition.

In this report, we revisit the role played by Arg-183, or its equivalent in the fold of HO enzymes, in determining the regioselectivity of heme hydroxylation. To this end, we performed studies with heme oxygenase from *Corynebacterium diphtheriae* (*cd*-HO), the sequence of which is closer to that of the mammalian enzymes than its bacterial HO counterparts, with both Arg-177 (Arg-183 in h-HO-1 and r-HO-1) and Lys-173 (Lys-179 in h-HO-1 and r-HO-1) being conserved. The crystal structure of *cd*-HO (PDB entry 1IW0) exhibits a similar arrangement of the residues near the heme propionates, where Lys-13 is positioned to hydrogen bond to the 6-propionate and both Tyr-130 and Arg-177 are located within 3 Å of heme propionate-7 (Figure 1B). We found that mutating Arg-177 to Asp or Glu results in the formation of 55% α- and 45% δ-biliverdin, respectively, and magnetic resonance spectroscopic studies revealed that the formation of δ-biliverdin is a consequence of in-plane heme disorder (two heme seatings).

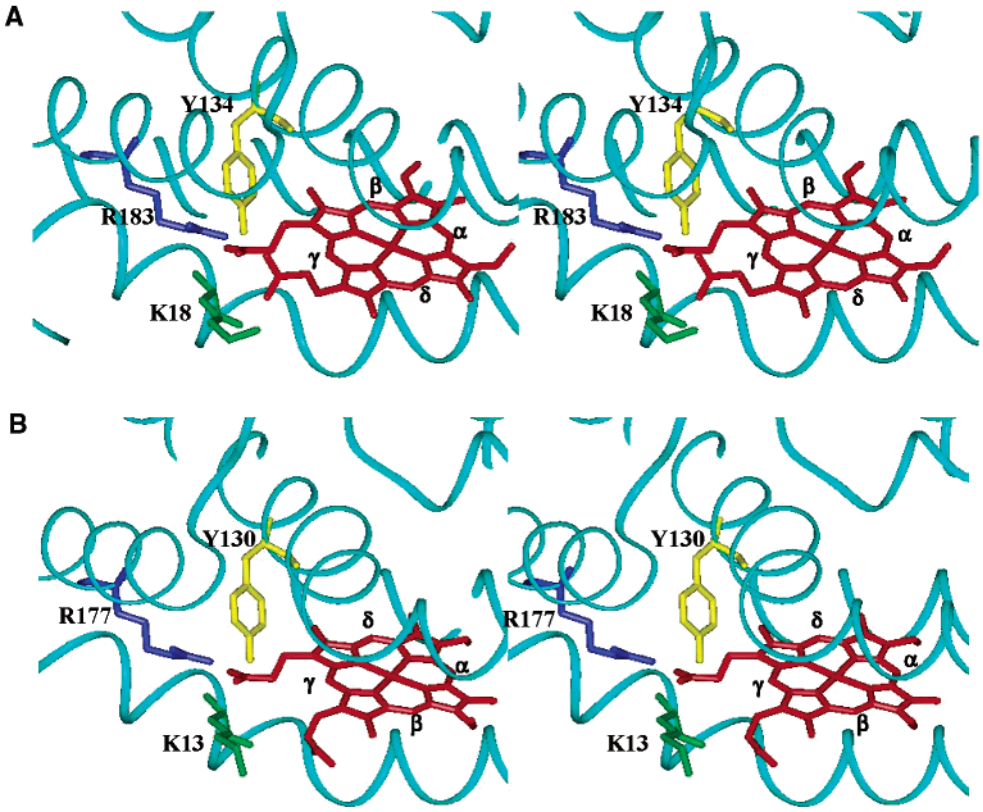

FIGURE 1: Stereoviews of the heme binding site in r-HO-1 (A) and *cd*-HO (B), illustrating the electrostatic and hydrogen bonding interactions between heme propionates and key residues nearby.

MATERIALS AND METHODS

General Methods. Plasmid purification, subcloning, and bacterial transformations were carried out as previously described (*24*). Mutagenesis was carried out by polymerase chain reaction using the Quickchange mutagenesis kit from Stratagene (La Jolla, CA). Oligonucleotides were designed to have melting temperatures (T_m) between 65 and 75 °C. All mutations were verified by DNA sequencing of the gene construct. DNA sequencing was carried out at the Biopolymer Laboratory, School of Medicine, University of Maryland. Deionized, doubly distilled water was used for all experiments. Oligonucleotides were obtained from Sigma-Genosys and used without further purification. All absorption spectra of the heme−HO complexes were recorded on a Carey Varian 1E UV spectrophotometer.

Bacterial Strains. Escherichia coli strain DH 5α [F′, *ara* D(*lac-proAB*) rpsL ø80d*lacZ*DM15 *hsd* R17] was used for DNA manipulation, and *E. coli* strain BL21 (DE3) pLysS [F^- *ompT hsdS*$_B$ ($r_B^- m_B^-$) *gal dcm* (DE3)] was used for expression of both the wild-type and mutant heme oxygenase constructs.

Expression and Purification of the Wild-Type and Mutant cd-HO Proteins. The wild-type and mutant *cd*-HO proteins were purified as previously described (*4*, *5*). A single colony of freshly transformed *E. coli* BL21 (DE3) pLysS cells was cultured overnight in 5 mL of LB medium containing 100 μg/mL ampicillin. The cells were subsequently subcultured into fresh LB−ampicillin medium (100 mL) and grown at 37 °C to mid-log phase. The cells were then subcultured (10 mL) into LB−ampicillin medium (1 L), and once the cells reached the mid-log phase, expression was induced by addition of isopropyl 1-thiol-D-galactopyranoside (IPTG) to a final concentration of 1 mM. The cells were grown further for 4−5 h at 30 °C and harvested by centrifugation (10000*g* for 20 min). Cells were lysed by sonication in 50 mM Tris-HCl (pH 7.8) containing 1 mM EDTA and 1 mM phenylmethanesulfonyl fluoride (PMSF). The cell suspension was then centrifuged at 27000*g* for 40 min. The soluble fraction was applied to a Sepharose-Q Fast Flow column (1.5 cm × 10 cm) previously equilibrated with 20 mM Tris-HCl (pH 7.5). The column was washed with 3 volumes of 20 mM Tris-HCl (pH 7.5) containing 50 mM NaCl. The protein was then eluted with the same buffer with a linear gradient of NaCl from 50 to 500 mM. The protein eluted at a concentration of 150 mM NaCl, and the peak fractions were pooled and dialyzed against 10 mM potassium phosphate (pH 7.4) (2 × 4 L) at 4 °C. The protein was then stored at −80 °C or reconstituted with heme. The heme−*cd*-HO complexes were prepared as described previously (*25*). Hemin was added to the purified HO proteins at a final 2:1 (heme:protein) ratio. The sample was then passed down a Sephacryl S-100 HR column (3.0 cm × 100 cm) following concentration on an Amicon filtration unit.

Absorption Spectroscopy of the Wild-Type and Mutant cd-HO Proteins. The UV−visible spectra of the wild-type HOs and their respective mutants were recorded in 20 mM Tris (pH 7.5). The Fe^{II}−CO spectra were obtained by saturating the solution with CO followed by the addition of a few grains of sodium dithionite. The $Fe^{II}-O_2$ complexes were obtained by passing the Fe^{II}−CO complexes through a Sephadex G-25 column (1 cm × 3 cm). The pK_a of the $Fe^{III}-H_2O$ to Fe^{III}−OH transition was measured from the pH-dependent changes in absorbance at 404 nm in 100 mM potassium phosphate buffer. The line was drawn by fitting the data to the

Henderson−Hasselbalch equation where 0% ionization was set at pH 6.5 and 100% at pH 10.5.

Reaction of the Heme−cd-HO Complexes with NADPH Cytochrome P450 Reductase or Ascorbate. The reaction of the heme−HO complexes in the presence of NADPH reductase or ascorbate was carried out as previously described (*3*, *4*). Purified human cytochrome P450 reductase was added to the heme−HO complex (10 μM) at a reductase:HO molar ratio equal to 3:1 in a final volume of 1 mL of 20 mM Tris-HCl (pH 7.5). The reaction was initiated by the addition of NADPH in 10 μM increments to a final concentration of 100 μM. The spectral changes between 300 and 750 nm were monitored over a 30 min time period at 1 min intervals. Following completion of the reaction, the product was extracted for HPLC analysis as described below.

HPLC Analysis of the Heme−cd-HO Reaction Products. Following the reaction of the heme−*cd*-HO complexes with ascorbate or NADPH cytochrome P450 reductase, glacial acetic acid (20 μL) and 3 M HCl (20 μL) were added to the reaction mixture (1 mL) before it was extracted into chloroform. The organic layer was washed with distilled water (3 × 1 mL) and the chloroform layer removed under a stream of argon. The resultant residue was dissolved in 1 mL of 4% sulfuric acid in methanol and esterified for 12 h at room temperature. The esters were diluted (4-fold) with distilled water and extracted into chloroform. The organic layer was washed further with distilled water and dried over sodium sulfate. The chloroform was again removed under a stream of argon. The residue was dissolved in HPLC solvent prior to HPLC analysis. The samples were analyzed via reverse phase HPLC on an ODS-AQ C18 (S-5) (YMC, Inc., Wilmington, NC) column (3.0 mm × 250 mm) eluted with an 85:15 (v/v) methanol/water mixture at a flow rate of 0.4 mL/min. The eluant was monitored at 380 nm, and the biliverdin standards eluted in the following order: α (11.9 min), β (13.9 min), δ (14.8 min), and γ (18.5 min).

Preparation of HOs Reconstituted with ^{13}C-Labeled Heme. ^{13}C-labeled δ-aminolevulinic acids (ALA) were used as biosynthetic precursors for the preparation of protoheme IX (heme). [3-^{13}C]-δ-Aminolevulinic acid ([3-^{13}C]ALA), [5-^{13}C]-ALA, and [1,2-^{13}C]ALA were synthesized utilizing methods described previously (*26*). Heme labeled with ^{13}C was obtained utilizing a previously reported methodology (*27*), which was developed to take advantage of the fact that the first committed precursor in heme biosynthesis is δ-aminolevulinic acid (ALA) (*28*, *29*). Thus, ^{13}C-labeled heme, which is biosynthesized in *E. coli* upon addition of suitably labeled ALA, is trapped by simultaneously expressing rat liver outer mitochondrial membrane cytochrome b_5 (OM cyt b_5) (*27*). The details of the biosynthetic protocol, which entail the expression and purification of OM cyt b_5 harboring ^{13}C-labeled heme, have been presented previously (*30*). Reconstitution of HO with ^{13}C-labeled heme entails the removal of the isotopically labeled macrocycle from OM cyt b_5, followed by the formation of the heme−HO complex. A typical protocol used to extract ^{13}C-labeled heme from OM cyt b_5 follows. Pyridine (15 mL) is added to 2.5 mL of 1 mM OM cyt b_5 in phosphate buffer (μ = 0.10, pH 7.0), while the temperature is kept at 4 °C. Slow addition of chloroform, typically 10−15 mL, results in the precipitation of the polypeptide, while the pyridine hemochrome is kept in the supernatant. The latter is subsequently separated from the denatured polypeptide by centrifugation, allowed to equilibrate at room temperature, and then dried over anhydrous $MgSO_4$. The desiccant is removed by filtration and the filtered pyridine/chloroform solution transferred to a round-bottom flask, where it is concentrated to dryness on a rotary evaporator. Finally, the solid is redissolved in 1.5 mL of dimethyl sulfoxide. HO is reconstituted with a freshly prepared solution of ^{13}C-labeled heme by titrating it into a 20 mL solution of 20 mM Tris containing ~2 μmol of HO until the A_{280}/A_{Soret} ratio no longer changes. The resultant solution containing the reconstituted enzyme is then incubated at 4 °C overnight and then purified by size exclusion chromatography with the aid of a Sephadex G-50 column [90 cm × 2.6 cm (inside diameter)] equilibrated and eluted with 10 mM phosphate buffer (pH 7.0) at 4 °C. Those fractions containing pure protein were concentrated in Amicon centrifugal concentrators to approximately 1 mL and then transferred to smaller Centricon concentrators to exchange the protein into deuterated phosphate buffer (at pH 7.4, not corrected for the deuterium isotope effect).

NMR Spectroscopy. ^{1}H and ^{13}C spectra were recorded on a Varian Unity Inova spectrometer operating at frequencies of 399.906 and 100.563 MHz, respectively. ^{1}H spectra were referenced to the residual water peak at 4.8 ppm, and ^{13}C spectra were referenced to an external solution of dioxane [60% (v/v) in D_2O] at 66.66 ppm. Proton spectra were acquired with presaturation of the residual water peak over 15K data points, with a spectral width of 30 kHz, an acquisition time of 250 ms, a relaxation delay of 200 ms, and 1024 scans. ^{13}C spectra were collected over 24K data points, with a spectral width of 35 kHz, an acquisition time of 150 ms, a relaxation delay of 25 ms, and 400 000 scans. HMQC spectra (*31*) were typically acquired with spectral widths of 20 kHz for ^{1}H and 35 kHz for ^{13}C and a relaxation delay of 200 ms. HMQC spectra obtained from samples containing HO reconstituted with heme labeled using [1,2-^{13}C]ALA as a heme precursor (see Figure 4A) were acquired with refocusing delays based on a $^1J_{CH}$ of 140 Hz, while data obtained from HO reconstituted with heme labeled using [5-^{13}C]ALA as the heme precursor (see Figure 4B) were acquired with a $^1J_{CH}$ of 180 Hz. Data were collected as an array of 2K × 128 points with 512 scans per t_1 increment and processed by zero filling once in t_2 and twice in t_1 to obtain an 8K × 8K matrix. This was apodized with a 90°-shifted squared sine bell function and Fourier transformed. WEFT NOESY (*32*, *33*) spectra were acquired with 20 kHz in both dimensions, 2K data points in t_2, 256 increments in t_1, 352 scans per t_1 increment, and (typically) a mixing time of 30 ms. The data were processed by zero filling in both dimensions to obtain an 8K × 8K matrix, apodized with a 90°-shifted squared sine bell function, and Fourier transformed. EXSY (*34*) data were acquired in a similar manner except that the mixing time was set to 20 ms.

RESULTS AND DISCUSSION

Expression, Purification, and Spectral Characterization of the Heme−cd-HO Complexes. The mutants were expressed and purified as described previously for the wild-type protein (*4*, *5*). All of the proteins were judged to be >95% pure by SDS−PAGE (data not shown). The Soret maxima of the resting state ($Fe^{III}-H_2O$) wild-type and mutant

Table 1: Characteristic Spectral (UV−vis) Features of the Wild-Type and Mutant Heme−*cd*-HO Complexes

enzyme	Soret maximum (nm)			visible bands (nm)			Soret extinction coefficient (mM^{-1} cm^{-1})
	Fe^{III}	$Fe^{II}-O_2$	$Fe^{II}-CO$	Fe^{III}	$Fe^{II}-O_2$	$Fe^{II}-CO$	
wild type	403	406	421	631	575/540	568/538	150
K13N	405	406	418	631[a]	573/536	567/536	186
Y130F	403	409	418	631[a]	574/540	567/536	163
K13N/Y130F	404	409	418	575/537[b]	572/536	567/536	121
K13N/Y130F/R177A	412	410	419	575/540[b]	574/537	568/536	253
R177A	405	410	418	630[a]	574/538	568/536	244
R177D	407	406	420	575/540[b]	567/545	570/539	165
R177E	409	413	418	575/539	573/539	567/536	181

[a] A fraction of low-spin complex was evident from the spectrum. [b] A complete low-spin heme was evident from the absorption spectrum.

cd-HO proteins are identical at 404 nm (Table 1), and the Soret maxima of the $Fe^{II}-CO$ complexes are at 418 nm, with the exception of the *cd*-HO K13A/Y130F/R177A mutant which is at 419 nm. The Soret maximum of the $Fe^{II}-O_2$ complexes ranged from 406 nm for the K16N mutant to 413 nm for the R177E protein (Table 1).

Plots relating the percentage of relative dissociation of the $Fe^{III}-H_2O$ complex to form the low-spin $Fe^{III}-OH$ species as a function of pH for wild-type and mutant *cd*-HO enzymes are shown in Figure 2B; the pK_a values obtained from fitting each of the plots to the Henderson−Hasselbalch equation are given in Table 2. It is apparent that the introduction of a carboxylate group at position 177 in *cd*-HO does not significantly alter the pK_a values, which are 9.1 (wild type), 9.4 (R177E), and 9.5 (R177D), despite the fact that the R177E and R177D mutants of *cd*-HO oxidize the heme to form 55% α- and 45% δ-biliverdin, respectively. Hence, the small change in the value of the pK_a for each of the mutants implies that the formation of δ-biliverdin is likely not a consequence of a significant change in the structure of the distal pocket, as was suggested previously (*23*) to explain the oxidation of heme to ∼30% δ-biliverdin by the R183D and R183E mutants of r-HO-1. It will be demonstrated below that the formation of δ-biliverdin catalyzed by the R177D and R177E mutants of *cd*-HO is a consequence of an in-plane rotation of the heme caused by electrostatic repulsion between the negative charge on one of the heme propionates and the negative charge on the side chain of residue 177 (residue 183 in r-HO-1).

Catalytic Turnover of the Heme−cd-HO Mutants. As previously reported for *cd*-HO, the degradation of heme in the presence of NADPH cytochrome P450 reductase yields α-biliverdin as the sole product of the reaction (Table 2) (*3*). When the single K13N or Y130F mutant of *cd*-HO was investigated, no change in regioselectivity was observed. This observation is in agreement with results obtained from studying the K16N and Y112F point mutants in *nm*-HO (unpublished results). However, in contrast to the K16N/Y112F double mutant of *nm*-HO, which catalyzed the formation of significant amounts of the δ-isomer, the regioselectivity of the K13N/Y130F mutant of *cd*-HO was not altered relative to that exhibited by wild-type *cd*-HO, yielding only the α-biliverdin isomer (Table 2). Examination of the crystal structures of r-HO-1 and *cd*-HO reveals the proximity of Arg-183 (r-HO-1) or Arg-177 (*cd*-HO) (panels A and B of Figure 1, respectively) to the carboxylate group of heme propionates. It is therefore likely that Arg at this position in the fold of HO plays an important role in orienting the heme within the active site. Hence, the altered regioselectivity exhibited by the K16A/Y112F double mutant of *nm*-HO can be explained by the fact that the crystal structure of *nm*-HO (*9*) revealed the absence of a residue equivalent to Arg-183 (r-HO-1) or Arg-177 (*cd*-HO) in the proximity of the heme propionates. To investigate whether Arg-177 participates in promoting the proper orientation of the heme in *cd*-HO, the K13N/Y130F/R177A triple mutant was constructed. This mutant carried out the degradation of heme to yield 60% δ-biliverdin and 40% α-biliverdin (Table 2).

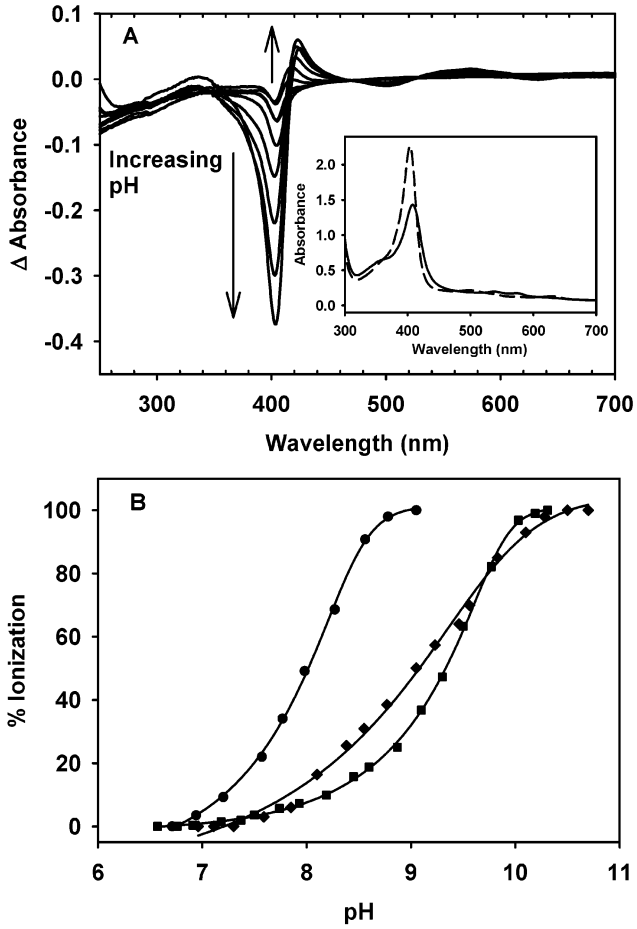

FIGURE 2: (A) Electronic absorption difference spectra of the R177D *cd*-HO complex as a function of pH. pH-dependent changes in absorption brought about by incremental addition of NaOH to a solution of $Fe^{III}-H_2O$ heme−*cd*-HO complexes in 20 mM Tris. The inset shows absolute spectra of the R177D *cd*-HO complex at pH 6.5 (− − −) and pH 10.5 (—). (B) The pK_a for the transition from the high-spin $Fe^{III}-H_2O$ to the low-spin $Fe^{III}-OH$ complex was monitored by following the absorption at 404 nm and by fitting the data to the Henderson−Hasselbalch equation: wild-type *cd*-HO (◆), *cd*-HO R177E (■), and *cd*-HO K13N/Y130F/R177A (●).

Table 2: Regioselectivity of the Heme Oxygenation and pK_a of the $Fe^{III}-H_2O$ to $Fe^{III}-OH$ Transition[a]

protein *cd*-HO	% biliverdin isomer α	β	δ	γ	pK_a[b]
wild type	100	0	0	0	9.1
K13N	95	0	5	0	9.4
Y130F	95	0	5	0	8.4
K13N/Y130F	95	0	5	0	8.8
R177D	55	0	45	0	9.5
R177E	45	0	55	0	9.4
R177A	90	5	5	0	9.2
K13N/Y130F/R177A	40	0	60	0	8.0

[a] The percentage of each isomer was obtained by integration of the peaks within each chromatogram. The reported values are averages obtained from five separate experiments. The standard deviation is ±5%. [b] The pK_a was determined from the change in absorbance at 404 nm and fit to the Henderson−Hasselbalch equation ($n = 1$).

Therefore, in contrast to *nm*-HO, in which Lys-16 and Tyr-112 exclusively control the orientation of the heme within the active site, in *cd*-HO and presumably in r-HO-1, Arg-177 and Arg-183, respectively, contribute significantly to maintaining the proper orientation of the heme within the active site. Evidence that supports this hypothesis is discussed in the following section.

NMR Spectroscopic Studies of the Influence Exerted by Arg-177 on the in-Plane Conformation of the Heme in cd-HO. The high-frequency portion of the ^{1}H NMR spectrum of cyanide-inhibited wild-type *cd*-HO (Figure 3a) is almost identical to the high-frequency portion of the spectrum reported for cyanide-inhibited h-HO-1 (*35*) and r-HO-1 (*36*) in that there is only one methyl resonance from the major heme orientational isomer (M) and one methyl resonance from the minor isomer (m) resolved from the diamagnetic envelope of resonances (M designates the major heme orientational isomer and m designates the minor orientational isomer that is related to M by a 180° rotation about the α−γ meso axis). We have previously suggested that this pattern of heme methyl resonances is characteristic of α-hydroxylating HO enzymes, where the proximal histidine−imidazole plane is aligned nearly parallel to the β−δ meso axis (*22*). When cyanide is added to the R177E mutant while the temperature is kept below 10 °C, one obtains the spectrum shown in Figure 3b, which displays two new peaks near 23 and 27 ppm in addition to the heme M and m resonances that are characteristic of α-hydroxylating HOs. If the sample is equilibrated at 20 and 30 °C, the corresponding spectra (spectra c and d of Figure 3, respectively) show that the intensity of the peaks near 23 and 27 ppm decreases and the M:m intensity ratio of the peaks increases at the more elevated temperatures. The fact that the M:m ratio increases with increased temperature suggests that at temperatures above 10 °C the minor orientational isomer (m) is converted into the major orientational isomer until a new equilibrium ratio is reached. To investigate the nature of the small peaks near 23 and 27 ppm, the R177E mutant was reconstituted with heme labeled with ^{13}C at the methyl carbons and cyanide was added while the solution was kept at 10 °C. In the corresponding spectrum (Figure 3e), the peaks near 23 and 27 ppm are clearly split into a $^1J_{CH}$ doublet, thus indicating that they correspond to heme methyl groups. These findings suggest that the small peaks near 23 and 27 ppm originate from an alternative conformation of the heme within the fold

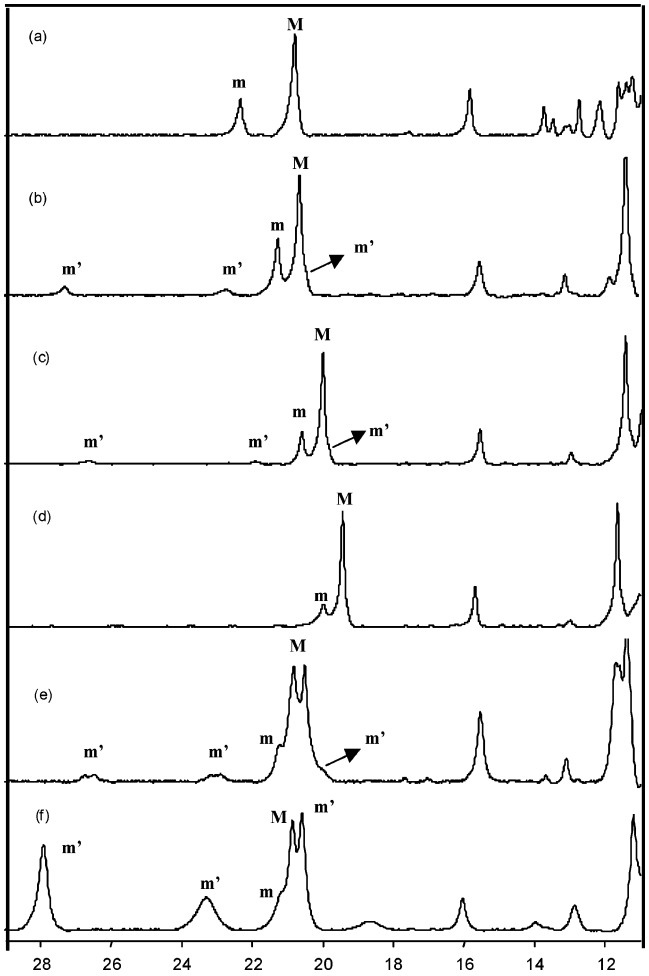

FIGURE 3: High-frequency portion of the ^{1}H NMR spectra of the cyanide-inhibited complexes of (a) wild-type *cd*-HO at 10 °C, (b) R177E *cd*-HO at 10 °C, (c) R177E *cd*-HO at 20 °C, (d) R177E *cd*-HO at 30 °C, (e) R177E *cd*-HO reconstituted with heme labeled with ^{13}C at all methyl carbons obtained at 10 °C, and (f) K13N/Y130F/R177A *cd*-HO at 10 °C. M and m represent the major and minor heme orientational isomers, respectively, related to one another by a 180° rotation about the α−γ meso axis. The alternative seating, m′, is related to m by an in-plane rotation of the macrocycle (see the text).

of the R177E polypeptide (m′). In fact, this behavior is reminiscent of that observed with mutants of *pa*-HO in which the heme was found to be in a dynamic equilibrium between two conformations (seatings) related to one another by an in-plane rotation of the heme within the polypeptide (*22*).

It is noteworthy that the concentration of the alternative seating m′ in the cyanide-inhibited enzyme decreases as the temperature is increased, and above 25 °C, it can go undetected if one is unaware of its presence. We will return to this point later in this report. It is also important to note that the line widths of the heme methyl resonances are not broadened excessively as would be expected if the rate of exchange between the two heme seatings was approximately equal to the NMR time scale. In addition, the chemical shifts of the heme methyl resonances corresponding to the wild-type heme seating are very similar to those exhibited by the wild-type protein at all temperatures, thus ruling out the possibility of fast exchange relative to the NMR time scale. Consequently, the observations summarized in spectra b−d of Figure 3 strongly suggest that the two heme seatings are

Table 3: ^{1}H NMR Chemical Shifts (parts per million) for the Cyanide Complexes of Wild-Type *cd*-HO and R177 Mutants at 10 °C

	wild type		R177A		R177E			R177D			K13N/Y130F/R177A		
position	^{1}H (M)[a]	^{1}H (m)[b]	^{1}H (M)[a]	^{1}H (m)[b]	^{1}H (M)[a]	^{1}H (m)[b]	^{1}H (m′)[c]	^{1}H (M)[a]	^{1}H (m)[b]	^{1}H (m′)[c]	^{1}H (M)[a]	^{1}H (m)[b]	^{1}H (m′)[c]
1-Me	4.32	6.60	4.29		4.36	5.34	19.94	4.79	5.48	20.50	4.55	5.49	20.46
3-Me	20.69	22.26	20.81	21.86	20.55	21.29	6.05	20.93	21.54	6.91	20.86	21.21	6.61
5-Me	7.91	8.15	7.64	8.56	7.52	7.78	27.47	7.68	7.58	27.24	7.82	8.52	27.72
8-Me	10.23	11.17	10.97	11.34	11.21	10.68	22.81	11.35	10.81	23.83	11.20	10.79	23.51
2-V$_\alpha$	15.79	13.45			15.29	13.14							
2-V$_\beta$	−5.06, −5.57	−6.24, −6.49			−5.04, −5.54	−6.76, −6.87							
4-V$_\alpha$	9.71				9.76								
4-V$_\beta$	0.84, 1.19	−0.18, −0.72			0.47, 0.25	−0.75, −1.88							
meso-α	−4.75				−4.71	−4.99							
meso-*β*	7.79				7.46								
meso-*γ*													
meso-*δ*	6.78	6.65			6.67	6.58							
6P$_\alpha$	8.50, 7.79				9.64, 8.21	10.34							
6P$_\beta$	−0.92, −1.19	−0.69, −0.91			−2.10, −2.87	−0.77, −1.74							
7P$_\alpha$	9.68, 7.74				9.80, 9.14								
7P$_\beta$	0.49, −1.01	1.31, −0.32			0.32, −1.36	−1.73, −2.38							

[a] M is the major orientational isomer. [b] m is the minor orientational isomer. [c] m′ is the alternative seating related to m by an 85° in-plane rotation.

in slow exchange relative to the NMR time scale at all temperatures that were studied.

The ^{1}H NMR spectrum of the K13N/Y130F/R177A triple mutant of CN-bound *cd*-HO (*cd*-HO−CN), where all residues that make electrostatic or hydrogen bonding interactions with the heme propionates have been replaced, displays the same set of peaks observed with the R177E and R117D mutants, except that the peaks that originate from the alternative heme seating (m′) are more intense (Figure 3f). This observation, which is consistent with the presence of two heme seatings in the triple mutant, suggests that removal of the stabilizing contacts between the heme propionates and the polypeptide induces in-plane heme disorder, which is conducive to altered regioselectivity. It is therefore of interest to determine the angle of the in-plane rotation that relates the two heme seatings to ascertain the in-plane conformation of the heme seating corresponding to m′. To accomplish this goal, it is first necessary to unambiguously assign the heme resonances to their corresponding groups in the heme moiety. The results from these studies are described below.

Resonance Assignments. The NMR spectroscopic studies described herein have been conducted with low-spin, cyanide-inhibited enzymes. The resonance assignments are summarized in Tables 3 and 4. Unambiguous assignments of ^{1}H and ^{13}C resonances originating from the heme active site of wild-type and mutant *cd*-HO enzymes have been obtained by studying enzymes reconstituted with ^{13}C-labeled heme. The assignment of heme resonances is largely facilitated by judiciously labeling the heme macrocycle, which is accomplished by carefully positioning the ^{13}C label in the heme precursors used in the biosynthesis of labeled heme. We used [1,2-^{13}C]-*δ*-aminolevulinic acid ([1,2-^{13}C]ALA) as a heme precursor for the preparation of heme labeled at the four methyl, two vinyl-*β*, two propionate-*β*, and carbonyl carbons (Figure 4A); [5-^{13}C]ALA was used to prepare heme labeled at the meso carbons (Figure 4B), and [3-^{13}C]ALA was used to prepare heme labeled at the vinyl-α and propionate-α carbons (Figure 4C) (*16*, *27*, *30*, *37*).

The low-frequency portion of the one-dimensional ^{13}C NMR spectrum (^{1}H-coupled) obtained from R177E *cd*-HO−CN clearly shows that the heme methyl carbons resonate between −15 and −60 ppm (Figure 5). The HMQC spectrum clearly reveals eight cross-peaks, which permit the identification of ^{1}H resonances originating from major (M) and minor (m) isomers, regardless of the fact that most heme methyl ^{1}H resonances are located under the intense envelope of polypeptide signals. The high-frequency portion of the ^{13}C spectrum corresponding to the HMQC spectrum of Figure 5 (not shown) allows the identification of the vinyl-*β* and propionate-*β* resonances. Similar experiments conducted with a sample of R177E *cd*-HO−CN reconstituted with heme labeled at the heme propionate-α (P$_\alpha$) and heme vinyl-α (V$_\alpha$) carbons (see Figure 4C) allowed us to identify the corresponding ^{1}H and ^{13}C resonances (Figure S1 of the Supporting Information). Resonances originating from meso carbons and their corresponding hydrogens were identified with the aid of an HMQC spectrum obtained from a sample of R177E *cd*-HO−CN reconstituted with heme labeled as in Figure 4B. The carbon resonance corresponding to the *δ*-meso carbon (meso-C$_\delta$) is unique because it is the only meso carbon not bound to a ^{13}C enriched pyrrole-α carbon and is therefore not affected by a $^1J_{CC}$ coupling. Consequently, the meso-H$_\delta$ resonance, which is readily identified from the HMQC map (Figure S2 of the Supporting Information), serves as a good entry point for interpreting the NOESY

Table 4: ^{13}C NMR Chemical Shifts (parts per million) for the Cyanide Complexes of Wild-Type *cd*-HO and R177D at 10 °C

	wild type		R177E		
position	^{13}C (M)[a]	^{13}C (m)[b]	^{13}C (M)[a]	^{13}C (m)[b]	^{13}C (m′)[c]
1-Me	−15.12	−19.41	−15.82	−17.15	−45.41
3-Me	−48.82	−50.46	−50.26	−50.32	−15.77
5-Me	−22.28	−22.94	−22.41	−22.73	−60.14
8-Me	−25.67	−26.18	−29.30	−26.69	−53.87
2-V$_\alpha$			44.28		
2-V$_\beta$	187.82		185.58	185.92	
4-V$_\alpha$			78.42		
4-V$_\beta$	146.63	143.57	151.33	145.11	
meso-α	54.81		46.62	55.61	
meso-*β*	10.65		7.58		
meso-*γ*					
meso-*δ*	12.92		9.65	13.89	
6P$_\alpha$			−34.31	−39.15	
6P$_\beta$	120.09	128.11	112.41	145.10	
7P$_\alpha$			−43.25		
7P$_\beta$	139.64	123.26	138.97	120.36	

[a] M is the major orientational isomer. [b] m is the minor orientational isomer. [c] m′ is the alternative seating related to m by an 85° in-plane rotation.

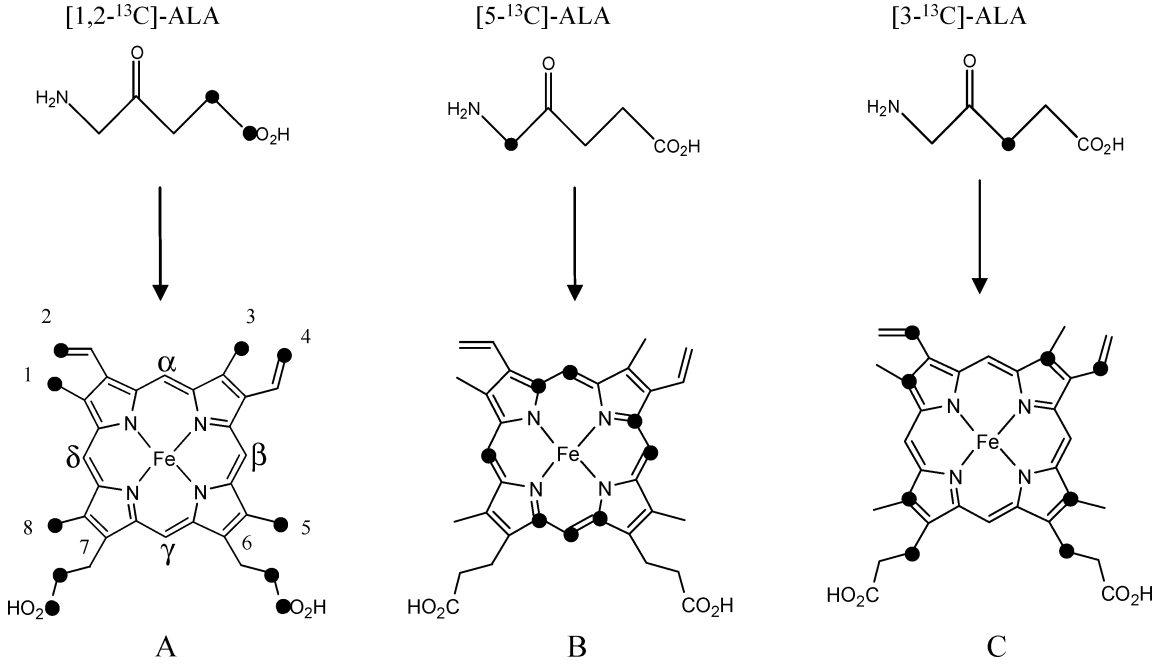

FIGURE 4: ^{13}C labeling patterns obtained when protoporphyrin IX is biosynthesized from (A) [1,2-^{13}C]ALA, (B) [5-^{13}C]ALA, and (C) [3-^{13}C]ALA.

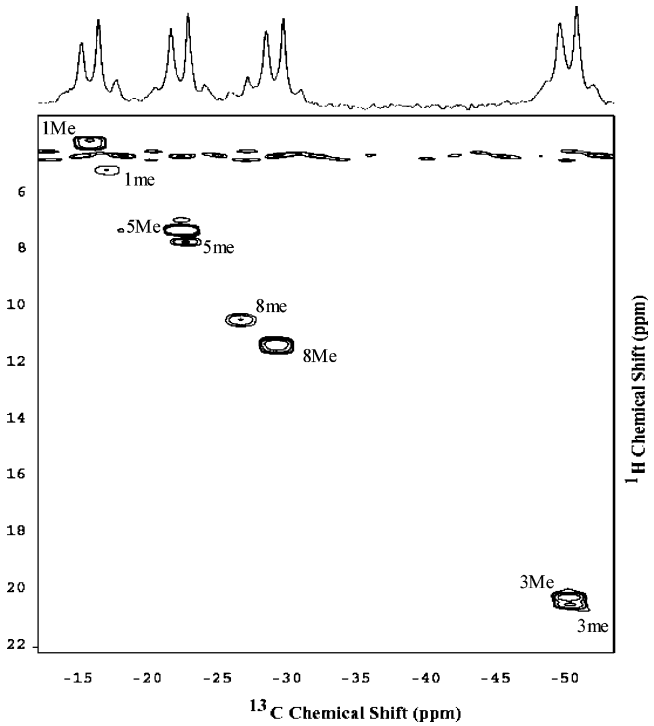

FIGURE 5: Low-frequency portion (10 °C) HMQC spectrum obtained from cyanide-inhibited R177E *cd*-HO reconstituted with heme derived from [1,2-^{13}C]ALA. The nondecoupled one-dimensional ^{13}C spectrum is shown to illustrate the $^{1}J_{CH}$ splittings. Cross-peaks labeled with an M originate from the major heme orientational isomer, and those from the minor orientational isomer are labeled with an m, which is related to M by a 180° rotation about the $\alpha-\gamma$ meso axis.

spectra. Analysis of the WEFT-NOESY spectrum of *cd*-HO R177E (Figure 6) allowed us to assign the previously identified resonances to their corresponding groups in the heme. For instance, the assignments of the major form M were obtained as follows. Meso C_δ facilitates the identification of meso-H_δ (6.67 ppm), highlighted with a blue circle in the NOESY spectrum (Figure 6A). The meso-H_δ resonance displays a correlation to heme methyl 1 (1Me) at 4.36 ppm, which in turn is correlated to a vinyl-β proton ($2V_\beta$) at −5.04 ppm. $2V_\beta$ at −5.54 ppm is correlated to $2V_\alpha$ at 15.29 ppm; the latter is correlated to meso-H_α at −4.71 ppm, and this meso hydrogen is correlated to the 3Me proton at 20.55 ppm, which in turn is correlated to $4V_\alpha$ at 9.76 ppm. The latter is correlated to one of the $4V_\beta$ protons at 0.47 ppm. This, in turn, is correlated to meso-H_β at 7.46 ppm. In Figure 6B, one can see the correlations between meso-H_δ (6.67 ppm) and 8Me at 11.21 ppm; the latter is correlated to the 7 propionate-α (7 P_α) protons at 9.14 and 9.80 ppm, which in turn are correlated to 7 P_β at −1.36 ppm, and the latter is correlated to the other 7 P_β at 0.32 ppm. The only heme methyl not yet assigned is that corresponding to 5Me. However, since the HMQC spectrum obtained with the enzyme reconstituted with heme labeled at all four methyl groups allowed the identification of all methyl carbon and corresponding proton resonances, the ^{1}H resonance at 7.52 ppm can be readily assigned to the 5Me group. The latter is correlated to one of the $6P_\alpha$ protons at 9.64 ppm, which in turn is correlated to the second $6P_\alpha$ proton at 8.21 ppm. Finally, both $6P_\alpha$ protons are correlated to the $6P_\beta$ protons at −2.10 and −2.87 ppm. The assignments corresponding to the minor form (m) and those corresponding to the M and m forms of the wild-type enzyme were obtained with a strategy identical to that described for the R177E mutant. The ^{1}H NMR spectra of the R177D mutant are almost identical to the spectra displayed by the R177E protein, and the ^{1}H NMR spectra of the R177A mutant are nearly identical to those obtained for wild-type *cd*-HO. Hence, the assignments corresponding to the R177D mutant were made by analogy to those of the R177E mutant, and the assignments corresponding to the R177A mutant were obtained by comparison to those of wild-type *cd*-HO.

In-Plane Conformation of the Heme. The orientation of the histidine−imidazole plane with respect to the axis along

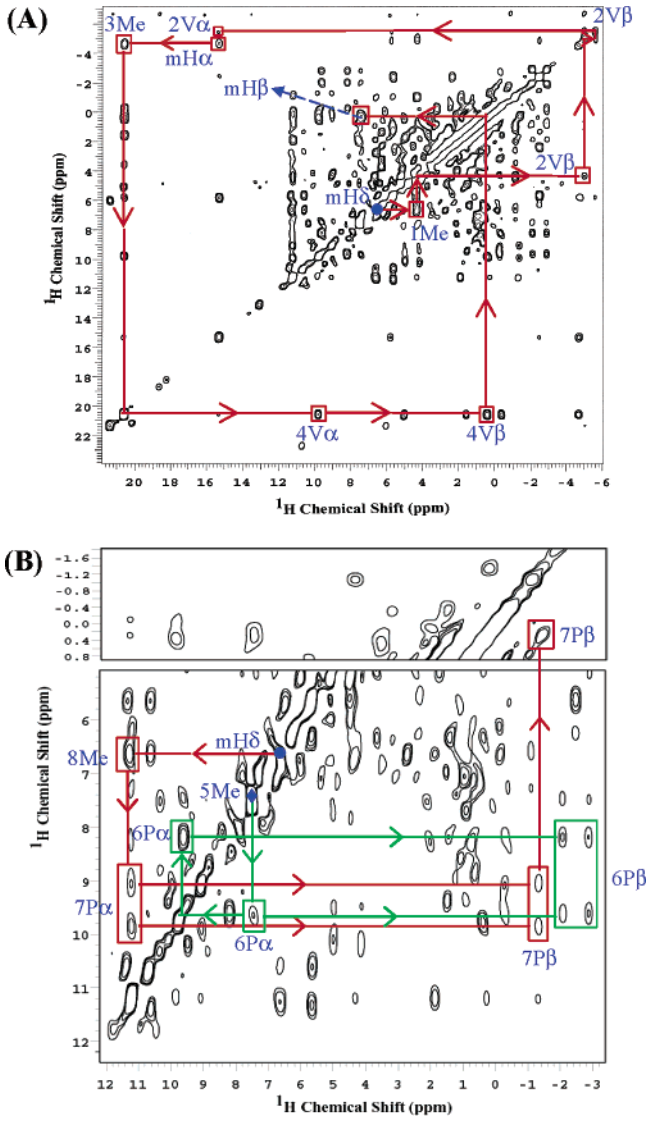

FIGURE 6: WEFT-NOESY spectrum of R177E *cd*-HO obtained at 10 °C. The arrows indicate the dipolar connectivities that permit the assignment of the resonances. In panel A, assignments start from meso-H_δ, highlighted with a blue circle. Thus, meso-H_δ → 1Me → $2V_\beta$ → $2V_\alpha$ → meso-H_α → 3Me → $4V_\alpha$ → $4V_\beta$ → meso-H_β. In panel B, assignments can be traced as follows: (red arrows) meso-H_δ → 8Me → $7P_\alpha$ → $7P_\beta$ and (green arrows) 5Me → one $6P_\alpha$ → second $6P_\alpha$ and $6P_\beta$.

pyrrole nitrogens II and IV, the angle ϕ in Figure 7, has been semiquantitatively correlated to the ^{1}H chemical shifts from heme methyl groups in low-spin ferrihemes coordinated by histidine and cyanide axial ligands (*38*). More recently, an expression containing heuristically determined parameters has been derived for bis-histidine and histidine−cyanide coordinated ferrihemes by fitting the shifts of cytochrome b_5, several cytochromes c_3, and histidine−cyanide systems (*39*). In the case of ferrihemes coordinated by axial histidine and cyanide ligands, the expression takes the form of eq 1

$$\delta_i = a \sin^2(\theta_i - \phi) + b \cos^2(\theta_i + \phi) + c \qquad (1)$$

where ϕ is the angle between the projection of the histidine−imadazole plane and the molecular x axis and θ_i is the angle between the axis along the ith methyl−Fe direction and the molecular x axis (see Figure 7) (*39*). Equation 1 permits a more quantitative estimation of the heme methyl chemical shifts; therefore, we have used this expression and the heuristic values of a (18.4 ppm), b (−0.8 ppm), and c (6.1 ppm) (*39*) to construct a plot (Figure 7) correlating the angle ϕ with the observed heme methyl chemical shifts. This plot is similar to that previously reported by Shokhirev and Walker (*38*) in that it provides a visual aid in the interpretation of chemical shifts with respect to axial ligand geometry but it permits a more quantitative estimation of the chemical shifts because the values in the plot of Figure 7 have been calculated with the heuristic expression (eq 1) derived by Bertini and Walker (*39*).

The discussion that follows is concerned with the interpretation of the heme methyl chemical shifts in the context of the plot in Figure 7. The ^{1}H resonance assignments (Table 3) indicate that the order of heme methyl resonances for the major heme orientational isomer (M) in wild-type *cd*-HO is as follows: 3-Me > 8-Me > 5-Me > 1-Me (20.69, 10.23, 7.91, and 4.32 ppm, respectively). This order suggests an angle ϕ of approximately 130°, which means that the plane of the proximal histidine is almost collinear with the $\beta-\delta$ meso axis. The corresponding chemical shifts originating from the minor isomer in wild-type *cd*-HO are identical in the order and very similar in magnitude to those originating from the major orientational isomer. This observation is in agreement with the fact that a 180° rotation about the $\alpha-\gamma$ meso axis results in a very similar value of ϕ (∼133°), as has been schematically illustrated in Figure 7. It is also apparent that the chemical shifts originating from the major and minor isomers in the R177D and R177E mutants (see Tables 3 and 4) are very similar to those corresponding to the wild-type enzyme. This indicates that the projection of the proximal histidine plane in these mutants is also approximately collinear with the $\beta-\delta$ meso axis in both heme orientational isomers. There is, however, an important difference between the NMR spectra of wild-type *cd*-HO and its R177D and R177E mutants, which was observed in the analysis of the NOESY maps obtained from the R177 mutants. These experiments demonstrated that the minor orientational isomer (m) of the R177D and R177E mutants is in slow exchange, relative to the NMR time scale, with an alternative heme seating (m′). The cross-peaks that stem from magnetization transfer between heme methyl resonances in the two interconverting heme seatings (Figure 8) of the R177E mutant can be summarized as follows:

wild-type m seating	alternative m′ seating
3-me (21.29 ppm)	3′-me (6.05 ppm)
8-me (10.68 ppm)	8′-me (22.81 ppm)
5-me (7.78 ppm)	5′-me (27.47 ppm)
1-me (5.34 ppm)	1′-me (19.94 ppm)

It is noteworthy that exchange cross-peaks were only detected for the minor orientational isomer (m), despite the fact that EXSY spectra were acquired with different mixing times, which ranged from 2 to 60 ms. These observations suggest that the major orientational isomer (M) is not in dynamic exchange between two heme seatings, or that this exchange occurs at a rate that cannot be detected by magnetization transfer experiments. It will be shown below that the more likely explanation is that the major orientational isomer is not in dynamic exchange between two seatings. However, before this issue can be addressed, it is necessary to establish

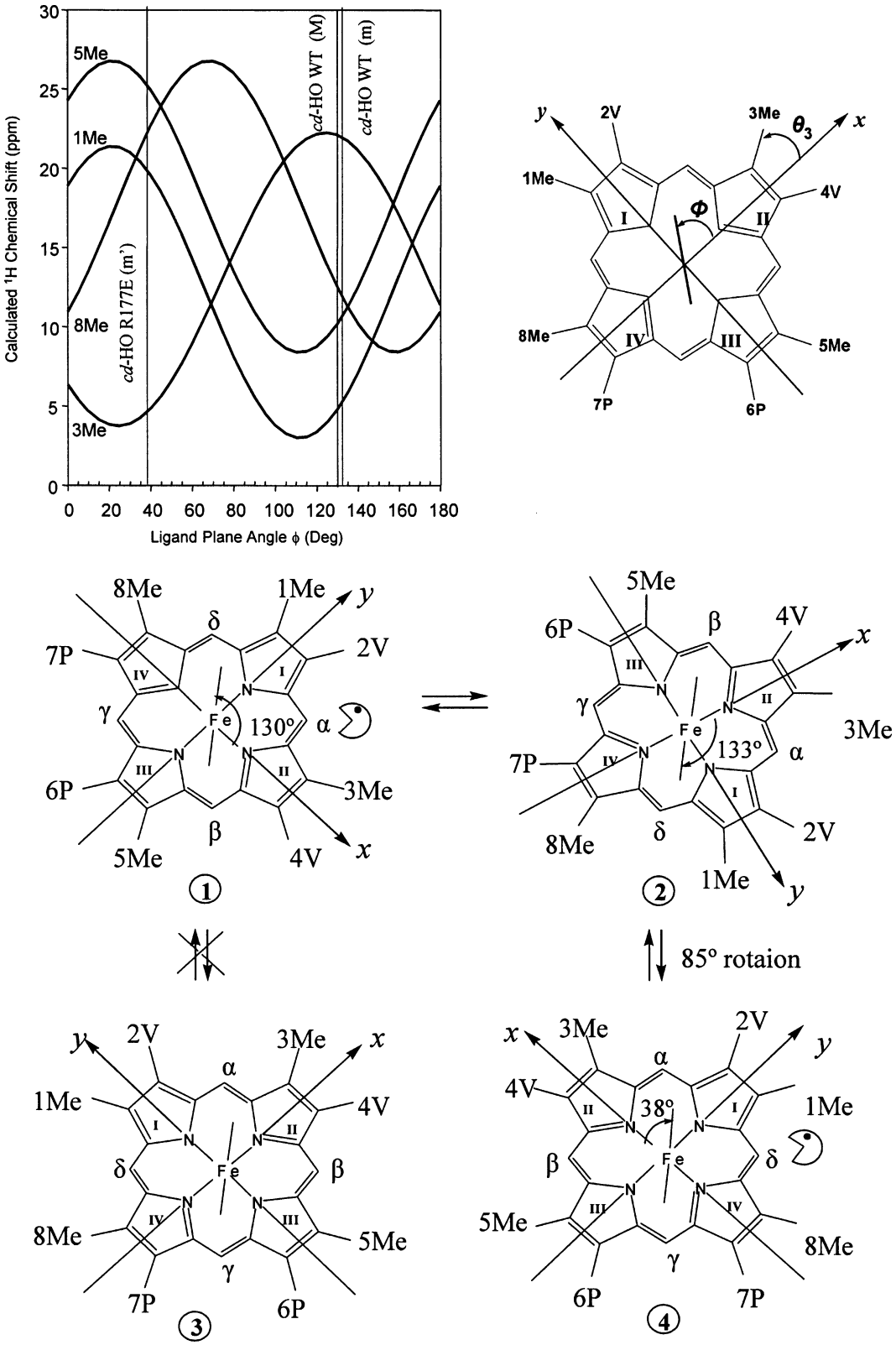

FIGURE 7: (Top) Right-handed coordinate system and nomenclature used for describing the projection of the His−imidazole plane onto the porphyrin ring. The *x* axis is aligned along the nitrogen atoms of pyrrole rings II and IV, the *y* axis along the nitrogen atoms of pyrrole rings I and III, and the *z* axis normal to the heme. The plot relating the dependence of the observed heme methyl shifts on the angle ϕ and the molecular *x* axis and the projection of the imidazole plane was calculated with the heuristic equation reported by Bertini and Walker (*39*), eq 1 in the text. θ_3 (23°) is the angle between the axis along the Fe-3 methyl direction and the molecular *x* axis. The θ_i angles for 1Me, 5Me, and 8Me relative to the *x* axis are as follows: $\theta_1 = \theta_3 + 90°$, $\theta_5 = \theta_3 - 90°$, and $\theta_8 = 180° - \theta_3$. (Bottom) Schematic representations of the in-plane orientation of the heme with respect to the proximal histidine−imidazole plane for heme orientational isomers M and m and for the in-plane rotated conformer m′.

the angle of in-plane rotation of the minor orientational isomer so that the NMR data can be discussed in the context of the different biliverdin isomers formed upon the oxidation of heme by the R177D and R177E mutants of *cd*-HO.

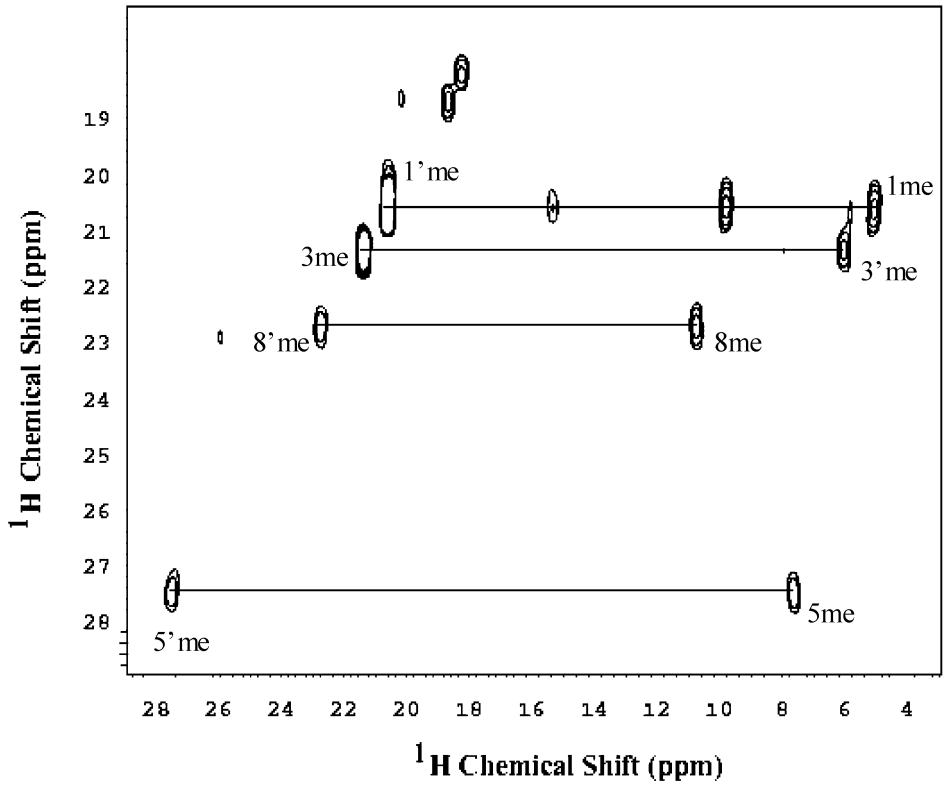

FIGURE 8: EXSY spectrum obtained from R177E *cd*-HO−CN at 10 °C. The heme methyl resonances arising from the minor orientational isomer m are labeled 1-me, 3-me, 5-me, and 8-me, and those from the alternative seating m′ are labeled 1′-me, 3′-me, 5′-me, and 8′-me.

The order of the heme methyl chemical shifts corresponding to the alternative heme seating (m′) in dynamic exchange with the seating corresponding to the minor orientational isomer (m) in the wild-type enzyme is as follows: 5′-me > 8′-me > 1′-me > 3′-me (27.47, 22.81, 19.94, and 6.05 ppm, respectively). The order and magnitude of these chemical shifts, interpreted in the context of the plot of Figure 7, suggest that the angle ϕ in the alternative heme seating is ~38°, which corresponds to an in-plane rotation of the heme of approximately 85° (shown schematically in Figure 7). The effect of this dynamic equilibrium on the regioselectivity of oxidative heme cleavage can be appreciated readily if analyzed in the context of the *cd*-HO fold. Thus, the stereoview of a model of the R177E mutant shown in Figure 9A depicts the heme orientational isomer (M) that is consistent with the X-ray crystal structure and solution NMR spectroscopic studies (*15*) of wild-type *cd*-HO. In comparison, Figure 9B illustrates a model of the minor orientational isomer (m), where the heme has been rotated 180° about the $\alpha-\gamma$ meso axis. It is apparent that rotation of the heme about the $\alpha-\gamma$ meso axis does not affect significantly the position of the α-meso carbon; hence, oxidation of the heme is expected to result in the formation of α-biliverdin from both heme orientational isomers. In contrast, if the heme in the minor orientational isomer rotates in-plane by approximately 85°, as can be predicted from the NMR spectroscopic studies, the δ-meso carbon will be placed within the fold of *cd*-HO in a position almost equivalent to that formerly occupied by the α-meso carbon (Figure 9C). Consequently, the δ-meso carbon should become susceptible to hydroxylation by the enzyme, a prediction that is consistent with the formation of δ-biliverdin upon enzymatic reaction of the R177E and R177D mutants.

The magnetization transfer experiments described above suggested that the major heme orientational isomer in the R177 mutants does not exhibit in-plane displacement. In fact, if similar in-plane displacement of the major orientational isomer is considered, it results in the placement of the β-meso carbon in the position formerly occupied by the α-meso carbon, which should be conducive to the formation of β-biliverdin. Thus, the fact that β-biliverdin is not detected upon enzymatic activity of the R177D and R177E mutants is consistent with the conclusion that the major orientational isomer does not exhibit a dynamic equilibrium between two heme seatings, as has been schematically depicted in Figure 7. The space filling representation of Figure 9D is shown to illustrate that the in-plane rotation of the heme that is conducive to seating m′ places the heme propionates in the solvent-exposed edge of the heme pocket. This seating of the heme (m′) is similar to that exhibited by heme oxygenase from *Pseudomonas aeruginosa* (*pa*-HO) (*22*). As is the case for m′ in *cd*-HO, the unusual seating of the heme in *pa*-HO places the δ-meso carbon where it is susceptible to hydroxylation, thus explaining the formation of δ-biliverdin as the major product of *pa*-HO activity (*22*).

It is important to point out that the NOESY spectrum of the R177E mutant reveals NOEs between a peptide signal at 0.35 ppm and the resonances corresponding to the 2-vinyl-α ($2V_\alpha$) proton (13.14 ppm) in m and the 8-methyl protons in m′ at 22.81 ppm (Figure 10A). The signal at 0.35 ppm also displays an NOE correlation to the resonance corresponding to the 3-methyl (3Me) group in heme seating M (20.55 ppm). In the crystal structure of *cd*-HO, one of the δ-methyl carbons of Leu-33 is located 3.80 Å from the heme 3-methyl carbon of seating M; hence, the signal at 0.35 ppm is tentatively attributed to one of the δ-methyl groups

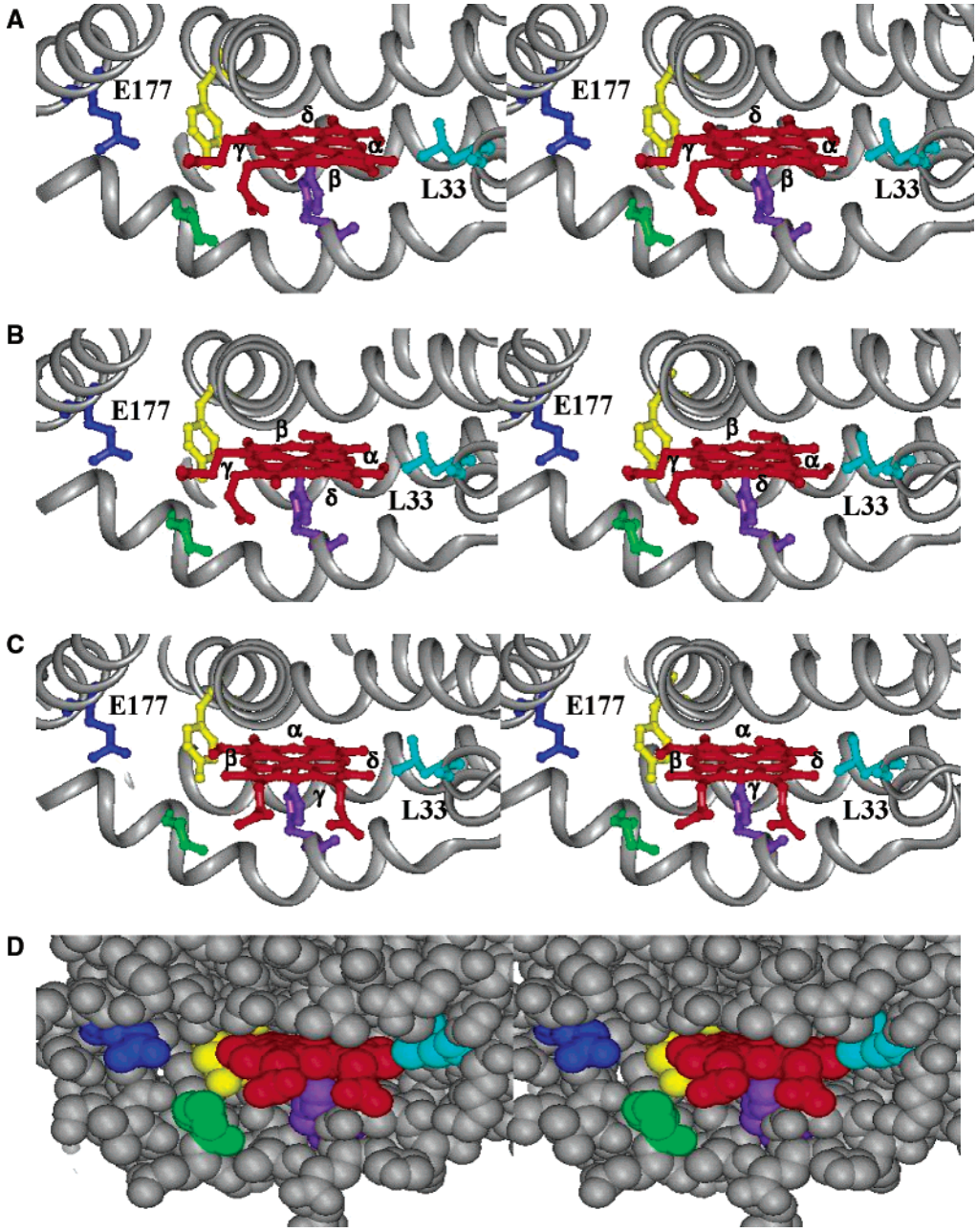

FIGURE 9: Stereo representations of a model of the heme active site of R177E *cd*-HO: (A) the major heme orientational isomer M, as found in the X-ray crystal structure (1IWO), (B) a model of the minor orientational isomer m, obtained by rotating the heme 180° about the $\alpha-\gamma$ meso axis, and (C) a model of the alternative seating of the heme m′, which is obtained by an 85° in-plane rotation of m. (D) Space filling representation of panel C illustrating that the heme propionates in m′ are exposed to the aqueous environment and do not experience electrostatic or steric repulsions.

of Leu-33 (see Figure 9A). Rotating the heme by 180° about the $\alpha-\gamma$ meso axis results in heme seating m, which places the $2V_\alpha$ proton in a position nearly equivalent to that occupied by the 3Me in M (Figure 9B). This is manifested in the NOE correlation between the signal at 0.35 ppm and the $2V_\alpha$ proton in m. Consequently, the NOE between the signal at 0.35 ppm and the 8-methyl group in heme seating m′ indicates that m and m′ are correlated by in-plane rotation (~85°) of the heme (Figure 9C) and not by rotation of the proximal histidine ligand.

The findings described above suggest that the presence of a negatively charged Asp or Glu side chain at position 177 introduces a repulsive interaction with one of the heme propionates, which forces an in-plane rotation of the heme and results in the formation of 45% δ- and 55% α-biliverdin. Consistent with this finding is the fact that mutating Arg-177 to Ala does not significantly alter the in-plane conformation of the heme, which is apparent from the fact that the R177A mutant produces 90% α-biliverdin and 5% of each of the β- and δ-isomers. However, the formation of only 90% α-biliverdin suggests that R177 does indeed contribute to stabilizing the in-plane conformation (seating) of the heme that places the α-meso carbon within the fold of *cd*-HO, where it is susceptible to hydroxylation. It was therefore of interest to probe the contribution of Lys-13 and Tyr-130, which also form electrostatic and hydrogen bonding interactions with the heme propionates, to the stability of the heme seating observed in wild-type *cd*-HO. The single K13N or Y130F or the double K13N/Y130F mutations do not result in significant changes in the seating of the heme, as is evident

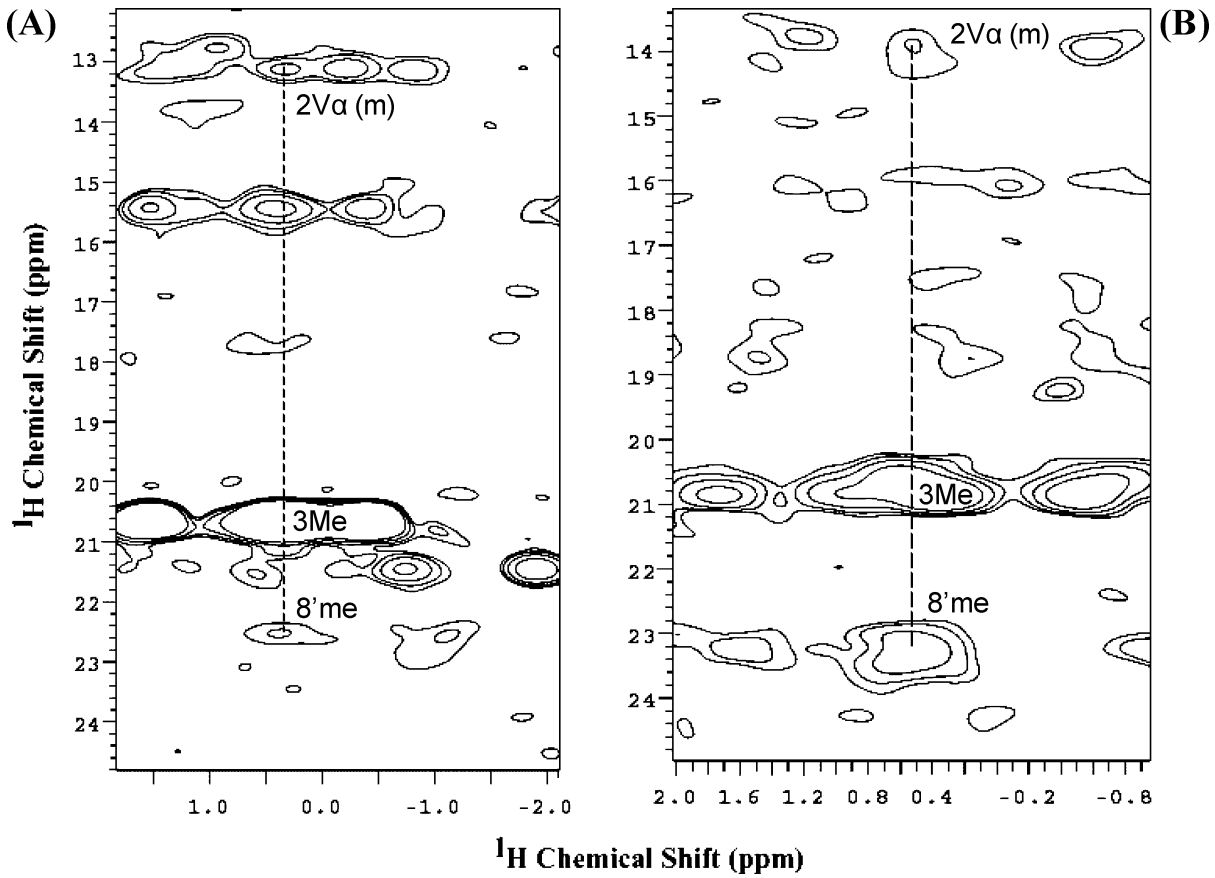

FIGURE 10: Portions of NOESY spectra obtained from (A) the R177E mutant of *cd*-HO illustrating NOEs between a polypeptide resonance at 0.35 ppm (tentatively attributed to H_δ of Leu-33) and the 2-vinyl-α proton in m and the 8-methyl protons in m′. These NOEs confirm in-plane rotation of m to acquire m′, as illustrated in panels B and C of Figure 9. (B) K13N/Y130F/R177A mutant of *cd*-HO showing NOEs between a polypeptide resonance at 0.51 ppm and the 2-vinyl-α proton in m and the 8-methyl protons in m′.

from the almost exclusive oxidation of the α-meso carbon (Table 2). On the other hand, the triple K13N/Y130F/R177A mutant catalyzes the formation of 40% α- and 60% *δ*-biliverdin, an observation that strongly suggests in-plane conformational disorder in this mutant similar to that exhibited by the R177D and R177E mutants of *cd*-HO (see above). In fact, it is apparent from the ^{1}H NMR spectrum of the K13N/Y130F/R177A mutant (Figure 3f) that this molecule exists as a mixture of two heme orientational isomers (M and m) and an alternative seating m′. Furthermore, the magnetization transfer experiment shown in Figure S3 of the Supporting Information indicates that the two heme seatings are related to one another by the following exchange cross-peaks:

wild-type m seating	alternative m′ seating
3-me (21.21 ppm)	3′-me (6.61 ppm)
8-me (10.79 ppm)	8′-me (23.51 ppm)
5-me (8.52 ppm)	5′-me (27.72 ppm)
1-me (5.49 ppm)	1′-me (20.46 ppm)

The chemical shifts originating from these two heme seatings, in the context of the plot in Figure 7, indicate that one of the seatings is almost identical to m in the wild-type enzyme ($\phi \sim 133°$). The alternative seating, with an angle ϕ of ∼38°, is almost identical to m′ in the R177D and R177E mutants. In-plane rotation of the heme is also manifested in a set of NOEs between a polypeptide signal at 0.51 ppm and the proton resonances corresponding to the $2V_\alpha$ proton in m and the 8Me protons in m′ (Figure 10B). It is therefore possible to conclude that the oxidation of heme to *δ*-biliverdin by the R177E, R177D, and K13N/Y130F/R177A mutants of *cd*-HO is a consequence of in-plane rotation of the heme.

In-Plane Heme Disorder and Regioselectivity of Meso Carbon Hydroxylation. The presence of two heme seatings in the cyanide-inhibited R177E mutant of *cd*-HO strongly suggests that the formation of 55% α- and 45% *δ*-biliverdin upon enzymatic activity is a consequence of the in-plane conformational disorder of the heme. However, before this conclusion can be reached with certainty, it is important to discuss some apparent inconsistencies between the relative proportion of the biliverdin isomers obtained experimentally and the corresponding proportion that can be calculated from the NMR spectrum of the cyanide-inhibited mutant. For instance, careful integration of the ^{1}H NMR spectrum of R177E *cd*-HO−CN obtained at ≤10 °C (Figure 3b) indicates that the solution contains ∼55% of the major orientational isomer (M), ∼40% of the minor orientational isomer (m), and ∼5% of the alternative seating (m′). Clearly, the concentration of m′ in the cyanide-inhibited protein is too small to account for the formation of ∼50% *δ*-biliverdin. The proportion of concentrations observed at 10 °C did not change over a period of several weeks when the sample was kept below 10 °C. On the other hand, if the temperature of the sample is increased to 20 °C, the integrals from the corresponding resonances (Figure 3c) indicate the presence of approximately 65% M, 33% m, and 2% m′, whereas at 30 °C (Figure 3d), m′ is almost undetectable and the solution

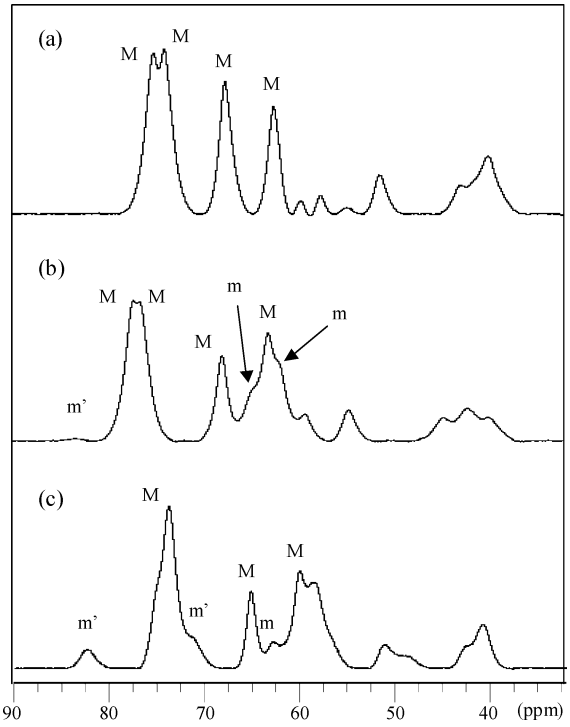

FIGURE 11: High-frequency portions of the ^{1}H NMR spectra of resting state ($Fe^{III}-H_2O$) *cd*-HO: (a) wild type, (b) R177E, and (c) K13N/Y130F/R177A.

contains approximately 70% M and 30% m. In addition, if CN^- is added to a solution of the R177E mutant at 20 °C, one obtains a spectrum very similar to that shown in Figure 3c; however, once the solution cools, the M:m:m′ ratio (∼65:33:2) does not change to the ratio of 55:40:5 observed when cyanide is added to the solution at ≤10 °C. These observations suggest that binding of CN^- in the distal pocket of *cd*-HO R177E at temperatures below 10 °C, which cause heme reorientation along the α−γ meso axis to be exceedingly slow, traps the proportion of heme orientational isomers [∼55:(45) M:(m + m′)] that coexist in the $Fe^{III}-H_2O$ resting state. In-plane heme rotation, on the other hand, continues to occur, as evidenced by the observation of exchange cross-peaks at 10 °C (Figure 8) and 4 °C (data not shown). These observations, however, do not make it possible to discern whether the proportion of in-plane conformers (∼40:5 m:m′) that is observed in the R177E CN mutant at ≤10 °C is representative of the corresponding proportion of in-plane conformers in the $Fe^{III}-H_2O$ resting state. Hence, in an attempt to gain additional insight into this issue, the enzymes were studied by ^{1}H NMR spectroscopy in their high-spin $Fe^{III}-H_2O$ resting state. Findings from these experiments are described below.

The high-frequency portions of the ^{1}H NMR spectra corresponding to wild-type *cd*-HO, R177E, and K13N/Y130F/R177A are shown as spectra a−c of Figure 11, respectively. The four peaks labeled with an M in the spectrum of wild-type *cd*-HO have been attributed to heme methyl groups on the basis of their relative intensity and chemical shifts. The ^{1}H NMR spectrum of the R177E mutant (Figure 11b) displays the same set of methyl M peaks in addition to new peaks, some of which may be attributed to heme methyl resonances from the minor isomer m. It is noteworthy that in addition to these peaks the spectrum of the R177E mutant reveals the presence of a broad peak with a comparatively low intensity at 83 ppm. We tentatively attribute this peak to a methyl resonance from the alternative seating m′ and in the following discussion describe additional evidence that supports this conclusion. This evidence stems from the ^{1}H NMR spectrum of the high-spin form of the K13N/Y130F/R177A triple mutant (Figure 11c), where the peak at ∼83 ppm is significantly more intense than that in the spectrum of R177E *cd*-HO. As discussed previously, the triple mutant oxidizes heme to produce 40% α- and 60% δ-biliverdin. Moreover, the ^{1}H NMR spectrum of the cyanide-inhibited form of this mutant (Figure 3f) indicates that the m′ seating, which places the δ-meso carbon where it is susceptible to hydroxylation, is significantly populated. Hence, it is not unreasonable to conclude that the peak at 83 ppm and possibly the peak at 71 ppm (which can be observed only in the spectrum of the triple mutant due to its relatively high intensity) indicate the presence of the m′ heme seating in the resting state of R177E and K13N/Y130F/R177A *cd*-HO.

The results obtained from studying the R177E mutant in its high-spin ($Fe^{III}-H_2O$) and low-spin ($Fe^{III}-CN$) forms indicate that the concentration of the heme seating that is conducive to δ-meso hydroxylation (m′) is low (∼5%) compared to the total yield of δ-biliverdin (55%). Thus, the fact that the oxidation of heme produces approximately 50% of each, α- and δ-biliverdin, can be interpreted as follows. (i) Most of the α-biliverdin is produced as a consequence of oxidizing the α-meso carbon in M. (ii) δ-Biliverdin is produced from the oxidation of the δ-meso carbon in m′. (iii) The hydroxylation of the α-meso carbon in m is nearly negligible. The nearly negligible oxidation of the α-meso carbon in m is probably a consequence of a combination of steric interactions between heme substituents and side chains in close contact and electrostatic repulsion between one of the heme propionates and E177. This combination of steric and electrostatic interactions may result in a slight in-plane rotation of the heme and slight conformational changes of distal helix residues that protect the α-meso carbon in m from reacting with the OH group of the $Fe^{III}-OOH$ complex. Hence, the dynamic equilibrium between m and m′ is conducive to the formation of ∼50% δ-biliverdin, despite the low equilibrium concentration of m′.

It is also interesting that M does not rotate in plane to populate M′, as evidenced by the absence of β-biliverdin upon enzymatic activity and by the lack of exchange cross-peaks corresponding to M in EXSY spectra of the R177E mutant. This reluctance to rotate despite the relative proximity of E177 may be explained by analyzing the crystal structure of wild-type *cd*-HO. This analysis reveals that rotating M by ∼85° to acquire M′ exchanges the 8-methyl group in M with the 2-vinyl group in M′, as shown in Scheme 1. In the crystal structure, the 8Me group in M experiences efficient hydrophobic packing with the side chains of Y130 and V131. Hence, when the 8Me group in M exchanges with the 2-vinyl group in M′, the latter will likely experience unfavorable hydrophobic interactions with the Y130 and V131, as shown in Scheme 1. In contrast, rotating m by a similar angle to produce m′ exchanges the 5Me group in m with the similarly sized 3Me group in m′. In addition, the 4-vinyl group in m′ takes the place of the larger 6-propionate group in m and thus is not expected to experience unfavor-

Scheme 1

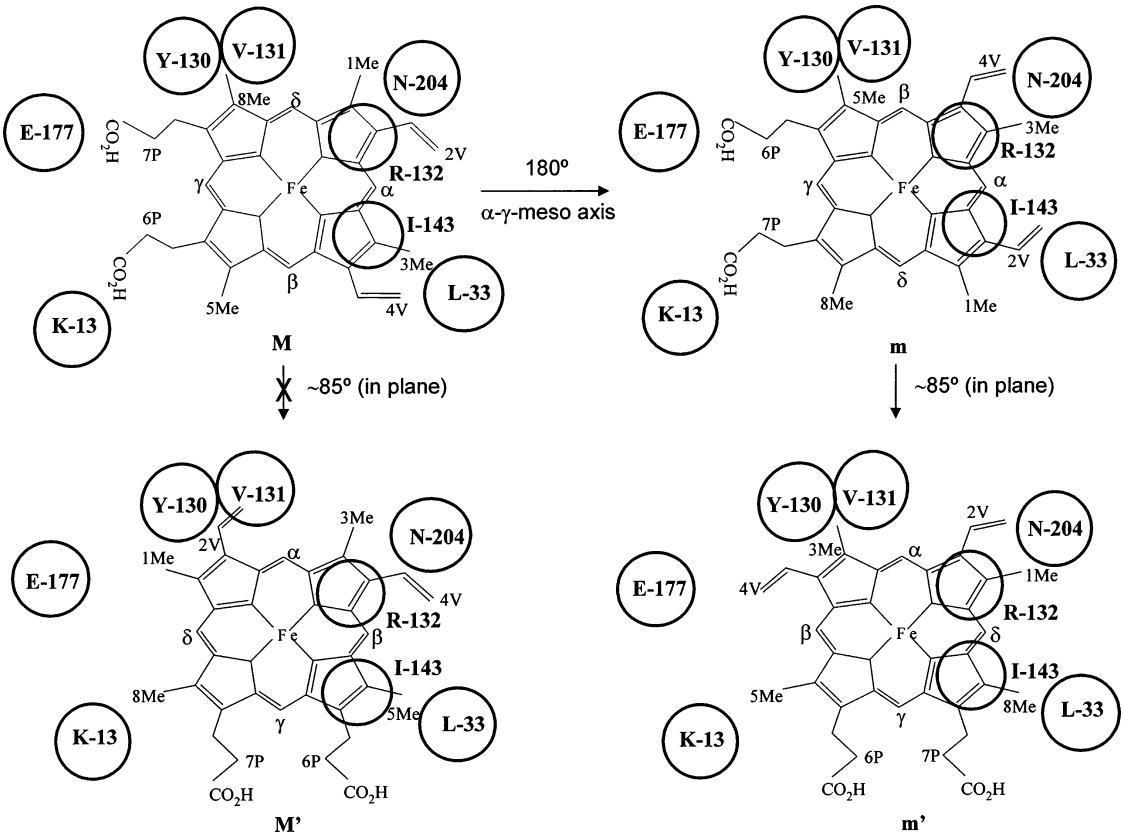

able packing interactions. As a consequence, there is a small (∼5%) population of m′, whereas M′ is negligibly populated.

Finally, we discuss the findings described above in the context of the conclusions reached in the study of the R183D and R183E mutants of r-HO-1 (*23*), which documented the first change in regioselectivity of heme hydroxylation by a heme oxygenase enzyme. The authors proposed two plausible mechanisms to explain the change in regioselectivity. (i) Electrostatic repulsion between R183D or R183E and one of the heme propionates forced the heme to rotate, thus placing the δ-meso carbon in place of the α-meso carbon, where it can be oxidized. (ii) The formation of a hydrogen bond between E183 and K179 was proposed to induce a rearrangement of S142 and K179, which would result in a change in the distal pocket that is conducive to the oxidation of the δ-meso position. The change in pK_a for the conversion of the aqua to the hydroxo complex observed in the R183E mutant was interpreted to be consistent with a change in structure of the distal pocket that leads to oxidation of the δ-meso carbon (*23*). In contrast, the large similarities between the ^{1}H NMR shifts of heme methyl resonances for wild-type r-HO-1, R183D r-HO-1, and R183E r-HO-1 were interpreted to indicate that the heme in the R183D and R813E mutants is not drastically rotated. It is interesting to point out, however, that despite the fact that mutating K179 resulted in a dramatic shift in the pK_a values of the mutants, no change in regioselectivity was observed (*24*). These data clearly indicate that there is no direct correlation between the apparent pK_a values and the altered regioselectivity observed in the R183E or R183D mutants, and imply that rearrangement of the distal hydrogen bonding network in the K179E or K179A mutant does not result in significant structural rearrangement of the distal pocket. On the other hand, these observations do not rule out the possibility that in the R183D and R183E mutants the altered regioselectivity is a consequence of in-plane rotation caused by electrostatic repulsion between the heme propionate and the carboxylate group introduced in the R183E mutant.

Inspection of the ^{1}H NMR spectra in the study reported by Zhou *et al.* (Figure S1 of the Supporting Information in ref *23*) reveals that the methyl resonances originating from the minor heme orientational isomer in the cyanide-inhibited R183D and R183E mutants of r-HO-1 (3-m and 8-m) are significantly broader than the corresponding resonances in the wild-type protein. This seems to indicate that in the cyanide-inhibited form the minor heme orientational isomer exhibits a dynamic behavior that is not shared by the major orientational isomer. In fact, in response to the comments made by Rice and Barker (http://pubs.acs.org/journals/jacsat/comments/ja0002868_rep1.html) about the paper by Zhou and co-workers (*23*), the authors indicate that because heme methyl resonances 3-m and 8-m in the R183D and R183E mutants of r-HO-1 are broader than the corresponding resonances in the wild-type enzyme, the heme in the minor isomer must be fluctuating rapidly, thus forming ∼30% δ-biliverdin. The results reported herein with the cyanide-inhibited R177D and R177E mutants of *cd*-HO demonstrate that it is possible to observe the alternative seating (m′) if CN^- is added to cold solutions (≤10 °C) of the mutant in its resting state and if the temperature is kept below 10 °C thereafter. However, if the temperature of the solution is increased above 10 °C, the peaks corresponding to the alternative seating (m′) disappear because the proportion of minor isomer (m + m′) becomes smaller as it is converted

into M. It is therefore not unreasonable to speculate that similar behavior of the CN^--inhibited form of the R183D and R183E mutants of r-HO-1 is the reason Zhou and coworkers (*23*) did not observe peaks corresponding to an alternative seating that is conducive to δ-hydroxylation.

Concluding Remarks. In this study, we have aimed to elucidate the role played by the heme propionates in properly orienting the heme within its binding site as a means of controling the regioselectivity of heme hydroxylation. We conclude that the initial orientation of the heme within the protein scaffold in *cd*-HO is primarily governed by interactions between the heme propionates and residues R177, K13, and Y130. These interactions position the heme such that the distal helix restricts access of the activated $Fe^{III}-OOH$ intermediate to all but the exposed α-meso carbon. Alteration or removal of the heme propionate interactions by site-directed mutagenesis allows the heme to rotate in plane and place the δ-meso carbon where is susceptible to being hydroxylated, which accounts for the altered regioselectivity. It is also interesting that suboptimal interactions between the heme propionates and the protein scaffold may result in poor reactivity, as suggested by the resistance to oxidation exhibited by the α-meso carbon of m in the R177E mutant. In addition to steric steering of the $Fe^{III}-OOH$ intermediate to a specific meso carbon, and on the basis of magnetic resonance studies conducted with models of the $Fe^{III}-OOH$ intermediate (*21*) and the hydroxide complex of heme oxygenase (*16*), we propose an electronic influence on meso carbon reactivity. In this model, the role of the extensive distal hydrogen bonding network (*14*, *15*) is to hydrogen bond to the coordinated ^-OOH ligand, thereby reducing its ligand field strength (*16*). As a consequence, the equatorial (porphyrin) ligand field strength is increased, which leads to nonplanar deformations of the macrocycle and the attainment of electronic configurations. These factors combined increase the electron and spin density at the meso positions and likely place the reactive meso carbon closer to the terminal OH group of the $Fe^{III}-OOH$ oxidizing species. Hence, the heme oxygenase reaction provides a new paradigm in heme protein chemistry in which a dynamic interplay of electronic and steric factors contributes to regioselectivity and reactivity.

SUPPORTING INFORMATION AVAILABLE

HMQC (10 °C) spectrum of R177E *cd*-HO reconstituted with heme derived from [3-^{13}C]ALA (Figure S1), HMQC (10 °C) spectrum obtained from R177E *cd*-HO reconstituted with heme derived from [5-^{13}C]ALA (Figure S2), and EXSY spectrum of K13N/Y130F/R177A *cd*-HO at 10 °C (Figure S3). This material is available free of charge via the Internet at http://pubs.acs.org.

REFERENCES

1. Tenhunen, R., Marver, H., Pimstone, N. R., Trager, W. F., Cooper, D. Y., and Schmid, R. (1972) Enzymatic Degradation of Heme. Oxygenative Cleavage Requiring Cytochrome P450, *Biochemistry 11*, 1716−1720.
2. Ortiz de Montellano, P. R., and Wilks, A. (2000) Heme Oxygenase Structure and Mechanism, *Adv. Inorg. Chem. 51*, 359−402.
3. Wilks, A., and Schmitt, M. P. (1998) Expression and characterization of a heme oxygenase (Hmu O) from *Corynebacterium diphtheriae*. Iron acquisition requires oxidative cleavage of the heme macrocycle, *J. Biol. Chem. 273*, 837−841.
4. Zhu, W., Wilks, A., and Stojiljkovic, I. (2000) Degradation of Heme in Gram-Negative Bacteria: the Product of the hemO Gene of Neisseriae Is a Heme Oxygenase, *J. Bacteriol. 182*, 6783−6790.
5. Ratliff, M., Zhu, W., Deshmukh, R., Wilks, A., and Stojiljkovic, I. (2001) Homologues of Neisserial Heme Oxygenase in Gram-Negative Bacteria: Degradation of Heme by the Product of the pigA Gene of *Pseudomonas aeruginosa*, *J. Bacteriol. 183*, 6394−6403.
6. Stojiljkovic, I., and Hantke, K. (1992) Hemin uptake system of *Yersinia enterocolitica*: similarities with other TonB-dependent systems in gram-negative bacteria, *EMBO J. 11*, 4359−4367.
7. Stojiljkovic, I., and Hantke, K. (1994) Transport of haemin across the cytoplasmic membrane through a haemin-specific periplasmic binding-protein-dependent transport system in *Yersinia enterocolitica*, *Mol. Microbiol. 13*, 719−732.
8. Zhu, W., Hunt, D. J., Richardson, A. R., and Stojiljkovic, I. (2000) Use of heme compounds as iron sources by pathogenic neisseriae requires the product of the hemO gene, *J. Bacteriol. 182*, 439−447.
9. Schuller, D. J., Zhu, W., Stojiljkovic, I., Wilks, A., and Poulos, T. L. (2001) Crystal Structure of Heme Oxygenase from the Gram-Negative Pathogen *Neisseria meningitidis* and a Comparison with Mammalian Heme Oxygenase, *Biochemistry 40*, 11552−11558.
10. Schuller, D. J., Wilks, A., Ortiz de Montellano, P. R., and Poulos, T. L. (1999) Crystal structure of human heme oxygenase-1, *Nat. Struct. Biol. 6*, 860−867.
11. Lad, L., Schuller, D. J., Shimizu, H., Friedman, J., Li, H., Ortiz de Montellano, P. R., and Poulos, T. L. (2003) Comparison of the Heme-free and -bound Structures of Human Heme Oxygenase, *J. Biol. Chem. 278*, 7834−7843.
12. Friedman, J., Lad, L., Deshmukh, R., Li, H., Wilks, A., and Poulos, T. L. (2003) Crystal Structures of the NO- and CO-bound Heme Oxygenase from *Nisseriae meningitidis*. Implications for O_2 Activation, *J. Biol. Chem. 278*, 34654−34659.
13. Li, Y., Syvitski, R. T., Auclair, K., Wilks, A., Ortiz de Montellano, P. R., and La Mar, G. N. (2002) Solution NMR Characterization of an Unusual Distal H-bond Network in the Active Site of the Cyanide-inhibited, Human Heme Oxygenase of the Symmetric Substrate 2,4-Dimethyldeuterohemin, *J. Biol. Chem. 277*, 33018−33031.
14. Li, Y., Syvitski, R. T., Auclair, K., Ortiz de Montellano, P. R., and La Mar, G. N. (2003) Solution ^{1}H NMR Investigation of Substrate-Bound, Cyanide-Inhibited Human Heme Oxygenase: Water Occupation of the Distal Cavity, *J. Am. Chem. Soc. 125*, 13392−13403.
15. Li, Y., Syvitski, R. T., Chu, G. C., Ikeda-Saito, M., and La Mar, G. N. (2003) Solution ^{1}H NMR Investigation of the Active Site Molecular and Electronic Structures of Substrate-Bound, Cyanide-Inhibited *HmuO*, a Bacterial Heme Oxygenase from *Corynebacterium diphtheriae*, *J. Biol. Chem. 278*, 6651−6663.
16. Caignan, G. A., Deshmukh, R., Zeng, Y., Wilks, A., Bunce, R. A., and Rivera, M. (2003) The Hydroxide Complex of *Pseudomonas aeruginosa* Heme Oxygenase as a Model of the Low-Spin Iron(III) Hydroperoxide Intermediate in Heme Catabolism: ^{13}C NMR Spectroscopic Studies Suggest the Active Participation of the Heme in Macrocycle Hydroxylation, *J. Am. Chem. Soc. 125*, 11482−11852.
17. Sugishima, M., Omata, Y., Kakuta, Y., Sakamoto, H., Noguchi, M., and Fukuyama, K. (2000) Crystal structure of rat heme oxygenase-1 in complex with heme, *FEBS Lett. 471*, 61−66.
18. Torpey, J., Lee, D. A., Smith, K. M., and Ortiz de Montellano, P. R. (1996) Oxidation of an α-Meso-Methyl-Substituted Heme to an α-Biliverdin by Heme Oxygenase. A Novel Heme Cleavage Reaction, *J. Am. Chem. Soc. 118*, 9172−9173.
19. Torpey, J., and Ortiz de Montellano, P. R. (1996) Oxidation of the meso-methylmesoheme regioisomers by heme oxygenase. Electronic control of the reaction regiospecificity, *J. Biol. Chem. 271*, 26067−26073.
20. Torpey, J., and Ortiz de Montellano, P. R. (1997) Oxidation of α-meso-formylmesoheme by heme oxygenase. Electronic control of the reaction regiospecificity, *J. Biol. Chem. 272*, 22008−22014.
21. Rivera, M., Caignan, G. A., Astashkin, A. V., Raitsimring, A. M., Shokhireva, T. K., and Walker, F. A. (2002) Models of the Low-Spin Iron(III) Hydroperoxide Intermediate of Heme Oxygenase: Magnetic Resonance Evidence for Thermodynamic Stabilization

of the d_{xy} Electronic State at Ambient Temperatures, *J. Am. Chem. Soc. 124*, 6077−6089.
22. Caignan, G. A., Deshmukh, R., Wilks, A., Zeng, Y., Huang, H., Moënne-Loccoz, P., Bunce, R. A., Eastman, M. A., and Rivera, M. (2002) Oxidation of Heme to *β*- and *δ*-biliverdin by *Pseudomonas aeruginosa* Heme Oxygenase as a Consequence of an Unusual Seating of the Heme, *J. Am. Chem. Soc. 124*, 14879−14892.
23. Zhou, H., Migita, C. T., Sato, M., Sun, D., Zhang, X., Ikeda-Saito, M., Fujii, H., and Yoshida, T. (2000) Participation of Carboxylate Amino Acid Side Chain in Regiospecific Oxidation of Heme by Heme Oxygenase, *J. Am. Chem. Soc. 122*, 8311−8312.
24. Sambrook, J., Fritsch, E. F., and Maniatis, T. (1989) *Molecular Cloning: A Laboratory Manual*, Cold Spring Harbor Laboraory Press, Plainview, NY.
25. Wilks, A., and Ortiz de Montellano, P. R. (1993) Rat liver heme oxygenase. High level expression of a truncated soluble form and nature of the meso-hydroxylating species, *J. Biol. Chem. 268*, 22357−22362.
26. Bunce, R. A., Shilling, C. L., III, and Rivera, M. (1997) Synthesis of [1,2-^{13}C]- and [2,3-^{13}C]-Labeled *δ*-Aminolevulinic Acid, *J. Labelled Compd. Radiopharm. 39*, 669−675.
27. Rivera, M., and Walker, F. A. (1995) Biosynthetic Preparation of Isotopically Labeled Heme, *Anal. Biochem. 230*, 295−302.
28. Warren, M. J., and Scott, A. I. (1990) Tetrapyrrole Assembly and Modification into the Ligands of Biologically Functional Cofactors, *Trends Biochem. Sci. 15*, 426−431.
29. Scott, A. I. (1993) How Nature Synthesizes Vitamin B_{12}: A Survey of the Last Four Billion Years, *Angew. Chem. 32*, 1223−1376.
30. Rivera, M., Qiu, F., Bunce, R. A., and Stark, R. E. (1999) Complete Isomer-Specific ^{1}H and ^{13}C NMR Assignments of the Heme Resonances of Rat Liver Outer Mitochondrial Membrane Cytochrome b_5, *J. Biol. Inorg. Chem. 4*, 87−98.
31. Summers, M. F., Marzilli, L. G., and Bax, A. (1986) Complete ^{1}H and ^{13}C Assignments of Coenzyme B_{12} through the Use of New Two-Dimensional NMR Experiments, *J. Am. Chem. Soc. 108*, 4285−4294.
32. Patt, S. L., and Sykes, B. D. (1972) Water Eliminated Fourier Transform NMR Spectroscopy, *J. Chem. Phys. 56*, 3182−3184.
33. Lankhorst, P. P., Wille, G., van Boom, J. H., Altona, C., and Haasnoot, C. A. G. (1983) Conformational Analysis of a Ribopentanucleoside Tretaphosphate in Aqueous Solution. A Two-Dimensional NMR Study at 500 MHz, *Nucleic Acids Res. 11*, 2839−2856.
34. Jeneer, J., Meier, B. H., Bachmann, P., and Ernst, R. R. (1979) *J. Chem. Phys. 71*, 4546−4553.
35. Hernandez, G., Wilks, A., Paolesse, R., Smith, K. M., Ortiz de Montellano, P. R., and La Mar, G. N. (1994) Proton NMR Investigation of Substrate-Bound Heme Oxygenase: Evidence for Electronic and Steric Contributions to Stereoselective Heme Cleavage, *Biochemistry 33*, 6631−6641.
36. Gorst, C. M., Wilks, A., Yeh, D. C., Ortiz de Montellano, P. R., and La Mar, G. N. (1998) Solution ^{1}H NMR Investigation of the Molecular and Electronic Structure of the Active Site of Substrate-Bound Human Heme Oxygenase: The Nature of the Distal Hydrogen Bond Donor to Bound Ligands, *J. Am. Chem. Soc. 120*, 8875−8884.
37. Rivera, M., and Caignan, G. A. (2004) Recent Developments in the ^{13}C NMR Spectroscopic Analysis of Paramagnetic Hemes and Hemoproteins, *Anal. Bioanal. Chem. 378*, 1464−1483.
38. Shokhirev, N. V., and Walker, F. A. (1998) The Effect of Axial Ligand Plane Orientation on the Contact and Pseudocontact Shifts of Low-Spin Ferriheme Proteins, *J. Biol. Inorg. Chem. 3*, 581−594.
39. Bertini, I., Luchinat, C., Parigi, G., and Walker, F. A. (1999) Heme Methyl ^{1}H Chemical Shifts as Structural Parameters in Some Low-Spin Ferriheme Proteins, *J. Biol. Inorg. Chem. 4*, 515−519.

BI035970O